

1 **Isotopic signatures of production and uptake of H<sub>2</sub> by soil**

2

3 Qianjie Chen<sup>1,2</sup>, Maria E Popa<sup>1</sup>, Anneke M Batenburg<sup>1,3</sup>, and Thomas Röckmann<sup>1</sup>

4

5 <sup>1</sup> Institute for Marine and Atmospheric research Utrecht, Utrecht University, The Netherlands

6 <sup>2</sup> Department of Atmospheric Sciences, University of Washington, Seattle, Washington, USA

7 <sup>3</sup> Department of Applied Physics, University of Eastern Finland, Kuopio, Finland

8

9

10

11

12

13

14

15

16

17

18

19

20

21

22

23 **Abstract:** Molecular hydrogen ( $H_2$ ) is the second most abundant reduced trace  
24 gas (after methane) in the atmosphere, but its biogeochemical cycle is not well  
25 understood. Our study focuses on the soil production and uptake of  $H_2$  and the  
26 associated isotope effects. Air samples from a grass field and a forest site in the  
27 Netherlands were collected using soil chambers. The results show that uptake  
28 and emission of  $H_2$  occurred simultaneously at all sampling sites, with strongest  
29 emission at the grassland sites where clover ( $N_2$  fixing legume) was present.  
30 The  $H_2$  mole fraction and deuterium content were measured in the laboratory to  
31 determine the isotopic fractionation factor during  $H_2$  soil uptake ( $\alpha_{soil}$ ) and the  
32 isotopic signature of  $H_2$  that is simultaneously emitted from the soil ( $\delta D_{soil}$ ). By  
33 considering all net-uptake experiments, an overall fractionation factor for  
34 deposition of  $\alpha_{soil} = k_{HD} / k_{HH} = 0.945 \pm 0.004$  (95% CI) was obtained. The  
35 difference in mean  $\alpha_{soil}$  between the forest soil  $0.937 \pm 0.008$  and the grassland  
36  $0.951 \pm 0.025$  is not statistically significant. For two experiments, the removal of  
37 soil cover increased the deposition velocity ( $v_d$ ) and  $\alpha_{soil}$  simultaneously, but a  
38 general positive correlation between  $v_d$  and  $\alpha_{soil}$  was not found in this study.  
39 When the data are evaluated with a model of simultaneous production and  
40 uptake, the isotopic composition of  $H_2$  that is emitted at the grassland site is  
41 calculated as  $\delta D_{soil} = (-530 \pm 40) \text{‰}$ . This is less deuterium-depleted than what is  
42 expected from isotope equilibrium between  $H_2O$  and  $H_2$ .

43

## 44 **1. Introduction**

45

46 H<sub>2</sub> is considered as alternative energy carrier to replace fossil fuels in the future.  
47 However, the environmental and climate impact of a potential widespread use  
48 of H<sub>2</sub> is still under assessment. Several studies suggested that the atmospheric  
49 H<sub>2</sub> mole fraction might increase substantially in the future due to the leakage  
50 during production, storage, transportation and use of H<sub>2</sub>, which could  
51 significantly affect atmospheric chemistry (Schultz et al., 2003; Tromp et al.,  
52 2003; van Ruijven et al., 2011; Warwick et al., 2004).

53

54 In the troposphere, H<sub>2</sub> has a mole fraction of about 550 parts per billion (ppb =  
55 nmol mol<sup>-1</sup>) and a lifetime of around 2 years (Novelli et al., 1999; Price et al.,  
56 2007; Xiao et al., 2007; Pieterse et al., 2011; 2013). H<sub>2</sub> can affect atmospheric  
57 chemistry and composition in several ways. Firstly, it increases the lifetime of  
58 the greenhouse gas methane (CH<sub>4</sub>) via its competing reaction with the hydroxyl  
59 radical (OH) (Schultz et al., 2003; Warwick et al., 2004). Additionally, H<sub>2</sub>  
60 affects air quality because it is an ozone (O<sub>3</sub>) precursor and indirectly increases  
61 the lifetime of the air pollutant carbon monoxide (CO) through competition for  
62 OH. In the stratosphere, H<sub>2</sub>O that is produced through the oxidation of H<sub>2</sub>  
63 increases humidity, which can result in increased formation of polar

64 stratospheric clouds and O<sub>3</sub> depletion (Tromp, et al., 2003), but this effect may  
65 be weaker than estimated initially (Warwick et al. 2004; Vogel et al., 2012).

66

67 The main sources of tropospheric H<sub>2</sub> are the oxidation of CH<sub>4</sub> and non-methane  
68 hydrocarbons (NMHC) (48%), biomass burning (19%), fossil fuel combustion  
69 (22%) and biogenic N<sub>2</sub> fixation in the ocean (6%) and on land (4%), while the  
70 main sinks are soil uptake (70%) and oxidation by OH (30%) (Pieterse et al,  
71 2013).

72

73 The biogenic soil sink of H<sub>2</sub> is the largest and most uncertain term in the global  
74 atmospheric H<sub>2</sub> budget. Conrad and Seiler (1981) assumed that the soil uptake  
75 of atmospheric H<sub>2</sub> is most likely due to consumption by abiotic enzymes, since  
76 there were no soil microorganisms known to be able to fix H<sub>2</sub> at the low  
77 atmospheric mole fraction at that time. This remained the basic hypothesis of  
78 many further soil uptake studies (Conrad et al., 1983; Conrad and Seiler, 1985;  
79 Ehhalt and Rohrer, 2011; Guo and Conrad, 2008; Häring et al., 1994; Smith-  
80 Downey et al., 2006). However, Constant et al. (2008a) were first to identify an  
81 aerobic microorganism (*Streptomyces* sp. PCB7) that can consume H<sub>2</sub> at  
82 tropospheric ambient mole fractions, and suggested that active metabolic cells  
83 could be responsible for the soil uptake of H<sub>2</sub> rather than extracellular enzymes.  
84 Further studies showed that uptake activity at ambient H<sub>2</sub> level is widespread  
85 among the streptomycetes (Constant et al., 2010) and it was postulated that high



86 affinity H<sub>2</sub>-oxidizing bacteria are the main biological agent responsible for the  
87 soil uptake of atmospheric H<sub>2</sub> (Constant et al., 2011). Khdhiri et al. (2015)  
88 suggested that the relative abundance of high affinity H<sub>2</sub>-oxidation bacteria and  
89 soil carbon content could be used as predictive parameters for the H<sub>2</sub> oxidation  
90 rate. Determining the dominant mechanism of the H<sub>2</sub> soil uptake activity is still  
91 an active area of research.

92

93 It has been shown that soil uptake of H<sub>2</sub> can coexist with soil production  
94 (Conrad, 1994). H<sub>2</sub> is produced in the soil during N<sub>2</sub> fixation (e.g. by bacteria  
95 living symbiotically in the roots of legumes such as clover or beans) and dark  
96 fermentation. Although the H<sub>2</sub> produced in the soil by e.g. N<sub>2</sub> fixation can be  
97 largely consumed within the soil, a significant amount of H<sub>2</sub> escapes to the  
98 atmosphere (Conrad and Seiler, 1979; 1980). Conrad and Seiler (1980)  
99 estimated that 2.4 to 4.9 Tg a<sup>-1</sup> of H<sub>2</sub> is emitted into the atmosphere through N<sub>2</sub>  
100 fixation on land.

101

102 One approach to better understand the sources and sinks of H<sub>2</sub> is to investigate  
103 the isotopic fractionation processes involved, which act as a fingerprint for H<sub>2</sub>  
104 emitted from different sources or destroyed by different sinks. The isotopic  
105 composition of H<sub>2</sub> is expressed as:

106

$$\delta(\text{D}, \text{H}_2) = \frac{R_{\text{sa}}}{R_{\text{VSMOW}}} - 1$$

107  
108 where  $R_{\text{sa}}$  is the D/H ratio of the sample  $\text{H}_2$  and  $R_{\text{VSMOW}} = (155.76 \pm 0.8)$  parts per  
109 million ( $\text{ppm} = \text{mmol mol}^{-1}$ ) is the same ratio of the standard material, Vienna  
110 Standard Mean Ocean Water (VSMOW) (De Wit et al., 1980; Gonfiantini et al.,  
111 1993). For brevity, we will use the notation  $\delta\text{D}$  ( $=\delta\text{D}(\text{D}, \text{H}_2)$ ) throughout the  
112 rest of this paper. The  $\delta\text{D}$  values are usually given in per mill ( $\text{‰}$ ). Recent  
113 studies showed that the global mean  $\delta\text{D}$  value of atmospheric  $\text{H}_2$  is about  $+130 \text{‰}$   
114 (Batenburg et al., 2011; Gerst et al., 2000, 2001; Rice et al., 2010).

115  
116 The HH molecule is consumed preferentially over HD during both OH  
117 oxidation and soil uptake, with OH oxidation causing a much stronger isotope  
118 fractionation effect. Only a few studies have investigated the soil uptake of  $\text{H}_2$   
119 with isotope techniques. Gerst and Quay (2001) carried out field experiments in  
120 Seattle, United States and found  $\alpha_{\text{soil}} (= k_{\text{HD}}/k_{\text{HH}})$  to be  $0.943 \pm 0.024$  ( $1\sigma$ ). Note  
121 that  $k_{\text{HD}}$  and  $k_{\text{HH}}$  are removal rate constants for HD and HH respectively. Rahn  
122 et al. (2002a) collected air samples from four forest sites in ecosystems of  
123 different ages in Alaska, United States, in July 2001, and obtained a similar  
124 average value ( $0.94 \pm 0.01$ ). They suggested that  $\alpha_{\text{soil}}$  depends on the forest  
125 maturity, with smaller fractionation for more mature forests. Since the more  
126 mature forests showed larger deposition velocity ( $v_d$ ) of  $\text{H}_2$ , they further

127 suggested that lower uptake rates involve greater isotopic fractionation ( $\alpha_{\text{soil}}$   
128 further from 1) than fast uptake rates. Rice et al. (2011) performed deposition  
129 experiments in Seattle and found  $\alpha_{\text{soil}}$  varying from 0.891 to 0.976, with a mean  
130 of 0.934. They found  $\alpha_{\text{soil}}$  to be correlated with  $v_d$ , with smaller isotope effects  
131 ( $\alpha_{\text{soil}}$  closer to 1) occurring at higher  $v_d$ , which agreed with the suggestion by  
132 Rahn et al. (2002a). In addition, unpublished experiments from Rahn et al.  
133 (2005) yielded  $\alpha_{\text{soil}} = 0.89 \pm 0.03$  in three upland ecosystems that were part of an  
134 Alaskan fire chronosequence. The data suggest that variability in the  
135 soil/ecosystem affects  $\alpha_{\text{soil}}$  but no significant variability of  $\alpha_{\text{soil}}$  with season was  
136 detected. Hitherto, only  $\alpha_{\text{soil}}$  values from studies in Seattle and Alaska are  
137 available, and values from other locations and ecosystems are needed to learn  
138 more about the factors influencing  $\alpha_{\text{soil}}$ .

139

140 The  $\delta D$  of  $H_2$  from various surface sources has been reported as about -290 ‰  
141 for biomass burning (Gerst and Quay, 2001; Haumann et al., 2013) and between  
142 -200 ‰ and -360 ‰ for fossil fuels combustion (Rahn et al., 2002b; Vollmer et  
143 al., 2012). So far no field studies have determined the isotopic composition of  
144 the  $H_2$  emitted from soil. Two laboratory studies examined the isotopic  
145 signature of  $H_2$  produced from  $N_2$  fixation. Luo et al. (1991) reported a  
146 fractionation factor  $\alpha_{H_2/H_2O} = R(D/H, H_2)/R(D/H, H_2O) = 0.448 \pm 0.001$  between  
147 the  $H_2$  produced from  $N_2$  fixation and the  $H_2O$  used to grow the  $N_2$ -fixing  
148 bacteria for *Synechococcus sp.* and  $0.401 \pm 0.002$  for *Anabaena sp.*, respectively.

149 Walter et al. (2012) reported  $\alpha_{\text{H}_2/\text{H}_2\text{O}} = 0.363 \pm 0.019$  for the  $\text{N}_2$ -fixing  
150 rhizobacterium *Azospirillum brasiliensis*. It has been proposed that  
151 microbiological  $\text{H}_2$  consumption and production could modify the thermal  
152 isotopic equilibrium between  $\text{H}_2$  and  $\text{H}_2\text{O}$  in low-temperature hydrothermal  
153 fluids (Kawagucci et al., 2010). Compared to the surface sources,  $\text{H}_2$  produced  
154 from  $\text{CH}_4$  and NMHC oxidation is isotopically strongly enriched in deuterium,  
155 with  $\delta\text{D}$  between +120 and +180 ‰ (Rahn et al., 2003; Röckmann et al. 2003a,  
156 Pieterse et al., 2011).

157

158 Here we report measurements of the isotopic fractionation factors of  $\text{H}_2$  during  
159 soil deposition at two different sites in the Netherlands, a forest and a grassland  
160 site. For the grassland site we also determine the apparent isotopic composition  
161 of the  $\text{H}_2$  that was simultaneously emitted from the soil during the experiment.

162

163

## 164 **2. Methods**

165

### 166 **2.1 Sampling**

167

168 Air samples were collected from a soil chamber at two locations in the  
169 Netherlands (Fig. 1): a grass field around the Cabauw tall tower (51°58' N,

170 4°55' E) and a forest site near Speuld (52°13' N, 5°39' E). Two types of ground  
171 cover (grass with and without clover) were sampled at Cabauw, while three  
172 types of forest (Douglas fir, beech and spruce) were selected in Speuld. More  
173 information about the soil and vegetation type can be found in Beljaars and  
174 Bosveld (1997) for the Cabauw site, and in Heij and Erisman (1997) for the  
175 Speuld site.

176

177 Flask samples were filled with air from a soil chamber, using a closed-cycle air  
178 sampler (Fig. 2). The soil chamber consisted of two parts: the chamber body  
179 with a metal base at the bottom that was inserted about 2 cm into the soil, and a  
180 removable transparent lid with two connections for air sampling. The chamber  
181 had a height of 40 cm, an area of 570 cm<sup>2</sup> and a volume of 22.8 L; the air inside  
182 was mixed by a fan. The sampler could hold four flasks installed in series,  
183 which could be bypassed independently; the flow and pressure in the flasks  
184 were controlled. The air was dried using Mg(ClO<sub>4</sub>)<sub>2</sub>. After passing through the  
185 flasks the air was returned to the soil chamber, which kept the pressure inside  
186 the chamber approximately constant during sampling.

187

188 Air samples were collected from the chamber in 1 L glass flasks at 0, 10, 20 and  
189 30 minutes after closing the chamber (time interval changed to 5 minutes in  
190 Speuld because of the faster uptake). The gas flasks (Normag, Ilmenau,  
191 Germany) were made of borosilicate glass 3.3 with O-ring-sealed stopcocks

192 made of PCTFE (Kel-F) and covered with a dark hose. Thorough tests have  
193 demonstrated that air samples with typical trace gas content are stable in these  
194 flasks (Rothe et al., 2004). In the beginning, the whole sampling unit (all lines,  
195 connections and flasks) was flushed with ambient air for about 10 minutes at a  
196 flow rate of  $2 \text{ L min}^{-1}$  and a pressure of 100 kPa, with all flasks open and the  
197 chamber lid open. This initial flushing process was designed to fill the flasks  
198 with background air. The air pressure inside the flasks was increased to 200 kPa  
199 (180 kPa for Speuld samples) by adjusting the flow control valve and the valves  
200 on two pressure gauges (Fig. 2) before chamber closing and then maintained  
201 constant during the whole sampling time. The flow rate was maintained at  $2 \text{ L}$   
202  $\text{min}^{-1}$  at ambient pressure and temperature with a rotameter and the pressure  
203 inside the chamber was maintained at 100 kPa during the whole sampling time.  
204 The temperature was not recorded during the sampling. After the initial flushing,  
205 the first flask was closed and then the chamber was closed as well. Afterwards,  
206 the air was flushed from the chamber through three flasks (the first flask was  
207 by-passed) and back to the chamber. After 10, 20 and 30 minutes, the second,  
208 third and fourth flasks were closed.

209  
210 A total of 36 sets of air samples were collected in Cabauw during summer (June,  
211 July and August) 2012 and 12 sets were collected in Speuld in September 2012.  
212 Each set contains four air samples. In total, 186 valid samples were analyzed for  
213  $\text{H}_2$  mole fraction and its deuterium content (6 were lost during sampling,

214 transportation and measurement). All the Speuld samples and about half of the  
215 Cabauw samples were further used for analysis in this study. The reason why 50%  
216 of the Cabauw experiments were not used is that these experiments showed  
217 neither strong H<sub>2</sub> emission nor H<sub>2</sub> uptake and the isotopic signals were weak.  
218 Most experiments were conducted with the 22.8 L volume soil chamber as  
219 described above, while 10 experiments were conducted with a larger automated  
220 soil chamber with a volume of 125 L and a height of 22.5 cm.

221

222

## 223 **2.2 Laboratory determination of H<sub>2</sub> mole fraction and deuterium** 224 **content of air samples**

225

226 The mole fraction and the  $\delta D$  of H<sub>2</sub> were measured with a gas chromatography  
227 isotope ratio mass spectrometry (GC/IRMS) setup (Rhee et al., 2004). For H<sub>2</sub>  
228 mole fractions, the laboratory working standards are linked to the MPI-2009  
229 scale (Jordan and Steinberg, 2011). The  $\delta D$  values of the laboratory reference  
230 gases are indirectly linked to mixtures of synthetic air with H<sub>2</sub> of known  
231 isotopic composition, certified by Messer Griesheim, Germany (Batenburg et al.,  
232 2011). Most of the samples collected from Cabauw were measured within two  
233 months after sampling, while the samples from Speuld were kept in a dark  
234 storage room for around four months before measurement.

235

236 The operational principle of the GC/IRMS system is to separate H<sub>2</sub> from the air  
237 matrix at low temperature (about 36 K) and measure the HH and HD content  
238 with a mass spectrometer. The measurement includes four main steps:

239

240 (1) A glass sample volume (750 ml) is evacuated and subsequently filled with  
241 sample air to approximately 700 mbar. This volume is then exposed to a cold  
242 head (36 K) of a closed-cycle helium compressor for 9 minutes. During this  
243 stage, all gases except H<sub>2</sub>, helium (He) and neon (Ne) condense.

244

245 (2) The remainder in the headspace of the cold head and sample volume is then  
246 flushed with He carrier gas to a pre-concentration trap where H<sub>2</sub> is collected on  
247 a 25 cm long, 1/8 inch OD (outside diameter) stainless steel tube filled with fine  
248 grains (0.2 to 0.5 mm) of 5 Å molecular sieve, for 20 minutes. The pre-  
249 concentration trap is cooled down to the triple point of nitrogen (63 K) by  
250 keeping it in a liquid N<sub>2</sub> reservoir that is further cooled down by pumping on the  
251 gas phase.

252

253 (3) After the collection of H<sub>2</sub>, the pre-concentration trap is warmed up to release  
254 the absorbed H<sub>2</sub>, which is then cryo-focused for 4 minutes on a capillary (25 cm  
255 long, 0.32 mm ID (inside diameter)) filled with 5 Å molecular sieve at 77 K.  
256 After that, the cryo-focus trap is warmed up to ambient temperature and the H<sub>2</sub>



257 sample is flushed with He carrier gas onto the GC column (5 Å molecular sieve,  
258  $\approx 323$  K) where H<sub>2</sub> is chromatographically purified from potential remaining  
259 interferences.

260

261 (4) In the end, the purified H<sub>2</sub> is carried by the He carrier gas via an open split  
262 interface (Röckmann et al., 2003b) into the IRMS for D/H ratio determination.

263

264 More details about the GC/IRMS system and measurement steps can be found  
265 in Rhee et al. (2004) and Röckmann et al. (2010). The data correction  
266 procedures and isotope calibration are similar to those described in Batenburg et  
267 al. (2011). Four reference gases were used to determine the  $\delta D$  values of the  
268 samples. Two of them (Ref-1 and Ref-2) with  $\delta D$  values of  $(+207.0 \pm 0.3) \text{‰}$   
269 and  $(+198.2 \pm 0.5) \text{‰}$  were calibrated and used previously in Batenburg et al.  
270 (2011). The other two new reference gases (Ref-3 and Ref-4) were calibrated  
271 versus Ref-1 and Ref-2. The  $\delta D$  value of Ref-3 was  $(-183 \pm 2.4) \text{‰}$ . Ref-4 was a  
272 frequently measured reference gas that was measured usually about 5 times per  
273 sequence of measurement, while other three reference gases were measured  
274 about 1 to 3 times per sequence of measurement. The  $\delta D$  value of Ref-4  
275 dropped linearly with time from  $-115 \text{‰}$  to  $-157 \text{‰}$  between 1 Jun 2012 and 15  
276 Feb 2013, while the other three reference gases were stable.

277

## 278 **2.3 Non-linearity of the GC/IRMS system**

279

280 Ideally, the  $\delta D$  of  $H_2$  measured with the GC/IRMS should not depend on the  
281 total amount of  $H_2$  used for analysis, but in practice a dependence of the isotopic  
282 composition on the amount of  $H_2$  is observed for low mole fractions. This is  
283 called non-linear behavior, and it is a particularly severe limitation for soil  
284 uptake studies, since the mole fraction in such samples can decrease by more  
285 than an order of magnitude. For comparison, in ambient background air the  $H_2$   
286 mole fraction variations are usually no more than 20%.

287

288 Experiments were carried out with different quantities of air from various  
289 laboratory reference bottles with known  $\delta D$  to determine a suitable correction  
290 for the non-linear behavior. The measured  $\delta D$  increases with the mass 2 sample  
291 peak area, which is proportional to the  $H_2$  quantity in the sample. In the peak  
292 area range of 0.2 Vs to 1 Vs this relation can be parameterized by a logarithmic  
293 function  $\delta D = 54.6 \ln (\text{peak area}/Vs) \text{ ‰}$ , which is used as correction function  
294 for the measurements at low peak areas (Fig. 3). The linearity correction  
295 introduces an additional uncertainty due to uncertainties in the logarithmic fit,  
296 particularly at low peak areas. The total assigned uncertainty for each  
297 measurement is calculated from the analytical and fitting uncertainty, as a  
298 function of peak area (Fig. 4). It is 2 ‰ for  $\ln (\text{peak area}/Vs)$  of 1.5 or more

299 (equivalent to more than 600 ppb H<sub>2</sub> in an air sample), but increases to 32 ‰  
300 when ln (peak area/Vs) drops to -1.6 (≈ 20 ppb H<sub>2</sub> in air sample). In total, the  
301 δD results of 18 Speuld samples that were measured at these low peak areas  
302 were corrected with this linearity correction. Possible additional systematic  
303 errors (a few ‰) may arise from uncertainties in the initially assigned δD  
304 values of the commercial calibration gases, changes of these values in the  
305 process of creating calibration mixtures with near-ambient H<sub>2</sub> concentration,  
306 and the calibration measurements themselves (Batenburg et al., 2011).

307

308

## 309 **2.4 Data evaluation**

310

311 Assuming first order kinetics for H<sub>2</sub> removal and a constant production rate  $P$   
312 over the course of a deposition experiment, the time evolution of the mole  
313 fraction  $c$  of non-deuterated H<sub>2</sub> (HH) inside the soil chamber can be expressed  
314 as:

315

$$\frac{d c}{d t} = P - k c \quad (1)$$

316

317 where  $k$  is the first order uptake rate constant of HH. For well-mixed air in the  
318 chamber,  $k = v_d/h$ , where  $v_d$  is the gross deposition velocity of H<sub>2</sub> and  $h$  is the

319 chamber height. The gross deposition velocity is the deposition velocity  
320 corrected for production, which is different from the net deposition velocity  
321 reported in some studies in the past that showed the effective uptake of H<sub>2</sub> from  
322 the atmosphere. The solution of Eq. (1) is of the form:

323

$$c = (c_i - c_e)e^{-kt} + c_e \quad (2)$$

324

325 where  $c$ ,  $c_i$  and  $c_e (= P/k)$  are the mole fractions of HH at time  $t$ , initially and at  
326 equilibrium, respectively. Therefore,  $P$  and  $k$  can be obtained by fitting an  
327 exponential function to the time evolution of HH inside the chamber. Similarly,  
328 we can obtain  $P'$  and  $k'$  from the time evolution of HD.

329

$$c' = (c'_i - c'_e)e^{-k't} + c'_e \quad (3)$$

330

331 where  $c'$ ,  $c'_i$ ,  $c'_e (= P'/k')$ ,  $P'$  and  $k'$  are the corresponding parameters for HD.

332

333 Equations (2) and (3) constitute the mass balance model that we used to analyze  
334 our data. When  $k$ ,  $k'$ ,  $P$  and  $P'$  have been determined,  $\alpha_{\text{soil}}$  and  $\delta D_{\text{soil}}$  can be  
335 calculated simply as:

336

$$\alpha_{\text{soil}} = \frac{k'}{k} \quad (4)$$

337

$$\delta D_{\text{soil}} = \frac{P'/P}{2R_{\text{VSMOW}}} - 1 \quad (5)$$

338

339 However, fitting an exponential curve to only four sample data yields relatively  
340 large errors for  $k, k', P$  and  $P'$ , which propagate to large errors for  $\alpha_{\text{soil}}$  and  $\delta D_{\text{soil}}$   
341 if they are determined directly from Eqs (4-5).

342

343 In Rice et al. (2011), Equations (2) and (3) were combined to calculate  $\alpha_{\text{soil}}$  in  
344 the presence of both source and sink of  $\text{H}_2$  using  $c_e$  and  $c_e'$  from the exponential  
345 fits:

346

$$\ln \frac{c' - c_e'}{c_i' - c_e'} = \frac{k'}{k} \ln \frac{c - c_e}{c_i - c_e} \quad (6)$$

347

348  $\alpha_{\text{soil}} = k'/k$  can be obtained by plotting  $\ln \frac{c' - c_e'}{c_i' - c_e'}$  versus  $\ln \frac{c - c_e}{c_i - c_e}$  and fitting a linear  
349 function. In the absence of soil emission ( $c_e = c_e' = 0$ ), Eq. (6) collapses to the  
350 well-known Rayleigh fractionation equation that is used to quantify the isotope  
351 fractionation during single stage removal processes in the absence of sources.

352

353 For the high emission measurements, where production overwhelms  
354 consumption, we use the relations  $c_e = P/k$  and  $c'_e = P'/k'$ , and obtain  $P'/P$  from  
355 the slope of  $c'_e \ln \frac{c'_i - c'_e}{c'_i - c'_e}$  against  $c_e \ln \frac{c - c_e}{c_i - c_e}$ . Then  $\delta D_{\text{soil}}$  is calculated from Eq. (5).

356

## 357 **2.5 Flask sampling model**

358

359 The advantage of sampling with the soil chamber system described in Section  
360 2.1 was that the pressure in the soil chamber stayed constant even when several  
361 large samples (2 L each) were taken. A disadvantage was that the volume of air  
362 inside the flasks (8 L of air in total) was considerable compared to the volume  
363 of air inside the soil chamber (22.8 L). This had two effects: (1) A significant  
364 part of the air was at each time separated from the chamber and thus from the  
365 soil production and uptake. (2) Because of the time lag to flush the samples, the  
366 air in a flask was not the same as the air in the chamber at the same time.

367

368 We built a flask sampling model to derive correction factors that take into  
369 account the influence of the flask sampling system. For a given combination of  
370 uptake and production rates, the model simulates the evolution of the  $\text{H}_2$  mole  
371 fraction in two configurations: the soil chamber alone, and the soil chamber plus  
372 four flasks as in our experiments. The model is described in detail in Appendix  
373 A. An example of a simulation is shown in Fig. 5. Compared to the situation

374 without flasks, there is a time lag in the decay of H<sub>2</sub> for both the chamber and  
375 the flasks after introducing four flasks in the model. The time lag for the second  
376 flask is about 2.5 minutes. It increases to 5 minutes for the third flask and is  
377 even longer for the fourth flask.

378

379 It is obvious that the sampling process strongly affects the uptake rate  $k_{\text{app}}$  and  
380 production rate  $P_{\text{app}}$  obtained from the direct flask measurements, so we  
381 corrected all  $k_{\text{app}}$  and  $P_{\text{app}}$  values with the correction coefficients derived from  
382 this flask sampling model (Appendix A). For a fixed chamber volume, sample  
383 pressure, flow rate and time interval of the flask collection that are all recorded  
384 for each experiment, the relationship between the actual uptake rate constant  
385  $k_{\text{true}}$  and apparent uptake rate constant  $k_{\text{app}}$  can be obtained (see Appendix A).  
386 Under the same sampling conditions for a fixed value of  $P_{\text{app}}$ , the relationship  
387 between actual production rate  $P_{\text{true}}$  and apparent production rate  $P_{\text{app}}$  depends  
388 on  $k_{\text{true}}$  (Fig 10b).

389

390 To evaluate the data, we first applied an exponential fit as in Eq. (2) to the  
391 measured HH mole fractions for the four flasks in each experiment and obtained  
392 *apparent* values  $k_{\text{app}}$ ,  $P_{\text{app}}$  and  $c_{e,\text{app}}$  from the fit parameters. Then we used the  
393 correction factors derived from the flask sampling model to retrieve true values

394  $k_{\text{true}}$  and  $P_{\text{true}}$  from the apparent values  $k_{\text{app}}$  and  $P_{\text{app}}$ . One can obtain  $k'_{\text{true}}$  and  $P'_{\text{true}}$   
395 by applying the same method to HD mole fractions inside four flasks.

396

397 To determine  $\alpha_{\text{soil}}$ , we plotted  $\ln \frac{c' - c'_{e,\text{app}}}{c'_1 - c'_{e,\text{app}}}$  versus  $\ln \frac{c - c_{e,\text{app}}}{c_1 - c_{e,\text{app}}}$  (Eq.6, Fig. 7) and

398 obtained  $\alpha_{\text{soil,app}}$  from the slope of the linear regression. Here,  $c$  and  $c'$  are HH

399 and HD mole fractions in each of the four flasks;  $c_1$  and  $c'_1$  are HH and HD

400 mole fractions of the first flask;  $c_{e,\text{app}}$  and  $c'_{e,\text{app}}$  are apparent HH and HD

401 equilibrium mole fractions obtained from the exponential fits of HH and HD

402 mole fractions inside the four flasks. We determined the relationship (Fig. 10c)

403 between  $\alpha_{\text{soil,true}}$  and  $\alpha_{\text{soil,app}}$  obtained from  $\ln \frac{c' - c'_{e,\text{app}}}{c'_1 - c'_{e,\text{app}}}$  versus  $\ln \frac{c - c_{e,\text{app}}}{c_1 - c_{e,\text{app}}}$  using the

404 flask sampling model (see Appendix A1.3). The correction coefficients for each

405 experiment are given in Table 3.

406

407 Similarly, we obtained  $P'_{\text{app}}/P_{\text{app}}$  by plotting  $c'_{e,\text{app}} \ln \frac{c' - c'_{e,\text{app}}}{c'_1 - c'_{e,\text{app}}}$  versus

408  $c_{e,\text{app}} \ln \frac{c - c_{e,\text{app}}}{c_1 - c_{e,\text{app}}}$  (Fig. 9), and calculated  $\delta D_{\text{soil,app}}$  by use of Eq. (5). Then we

409 retrieved  $\delta D_{\text{soil,true}}$  by use of the flask sampling model (Fig. 10d). The

410 corresponding correction coefficients for  $\delta D_{\text{soil,app}}$  for each net-emission

411 experiment are shown in Table 3. More information about the retrievals of

412  $\alpha_{\text{soil,true}}$  and  $\delta D_{\text{soil,true}}$  can be found in Appendix A.

413



414 Overall, the sampling effect on  $\delta D_{\text{soil}}$  is small (less than 22‰). This means that  
415 the flask sampling system strongly affects the temporal evolution of HH and  
416 HD individually (Fig. 5), and the uptake and production rates derived from flask  
417 measurements, but the effects on the computed isotopic signature of the source  
418 and sink are relatively small. More details and discussion of the flask sampling  
419 model corrections are provided in Appendix A.

420

421

## 422 **3. Results**

423

### 424 **3.1 Temporal evolution of H<sub>2</sub>, HD and $\delta D$**

425

426 Fig. 6 shows examples for the temporal evolution of H<sub>2</sub>, HD and  $\delta D$  in Cabauw  
427 and Speuld, with error estimates included. The errors for H<sub>2</sub> and HD are about 4%  
428 of the respective mole fraction. The error for  $\delta D$  ranges from 2 ‰ to 17 ‰.

429

430 Some of our Cabauw experiments show net soil emission of H<sub>2</sub> (upper panels)  
431 and some show net soil uptake (middle panels), while all Speuld experiments  
432 show net uptake of H<sub>2</sub> (lower panels). In the Cabauw net emission experiments,  
433 the increase in H<sub>2</sub> mole fractions is associated with a strong decrease in  $\delta D$ ,  
434 showing a strongly depleted H<sub>2</sub> source. However, the net uptake experiments at

435 Cabauw show also a decrease in  $\delta D$ , albeit smaller. In the Speuld experiments,  
436 the uptake of  $H_2$  is much faster; the  $\delta D$  increases in the beginning but then  
437 decreases again towards the end of the sampling, when the  $H_2$  mole fractions are  
438 low.

439

440 As mentioned in the introduction, soil uptake tends to increase  $\delta D$  while soil  
441 emission tends to decrease  $\delta D$  of  $H_2$ . The continuous decrease of  $\delta D$  with time  
442 in all Cabauw experiments and the eventual decrease of  $\delta D$  in all Speuld  
443 experiments clearly show that there is concurrent soil emission even with net  
444 uptake. Thus, the equilibrium  $H_2$  concentration in our experiments is not just a  
445 threshold concentration where microbial uptake stops, but the isotopic evolution  
446 shows that there is an active overlapping emission (Conrad, 1994).

447

448

### 449 **3.2 Emission and uptake strength of $H_2$**

450

451 The production rate  $P = P_{\text{true}}$  and uptake rate constant  $k = k_{\text{true}}$  were obtained by  
452 applying exponential fits to the temporal evolution of  $H_2$ , and applying the  
453 corrections derived from the flask sampling model (appendix A) to the  $P_{\text{app}}$  and  
454  $k_{\text{app}}$  obtained from the exponential fits (Fig. 6). The deposition velocity ( $v_d$ ),

455 production flux ( $F_p$ ), initial uptake flux ( $F_u$ ) and net flux at the beginning of the  
456 experiment ( $F_n$ ) were then calculated as follows:

457

$$v_d = kh \quad (7)$$

458

$$F_p = \frac{Ph}{V_M} \quad (8)$$

459

$$F_u = \frac{kc_1h}{V_M} \quad (9)$$

460

$$F_n = F_p - F_u \quad (10)$$

461

462 where  $h$ ,  $V_M$  and  $c_1$  are the chamber height, standard molar volume (=22.4 L  
463 mol<sup>-1</sup>) and H<sub>2</sub> mole fraction of the first flask, respectively. We note that with our  
464 method we derive  $v_d$  as deposition velocity for the gross uptake, unlike most of  
465 the results reported in the literature that just measured net uptake.

466

467 The strongest soil uptake occurs in the Speuld experiments (Table 1a), with a  
468 mean  $v_d$  of (0.17±0.02) (2 SE, n=12) cm s<sup>-1</sup> (SE represents standard error). On  
469 average, the Cabauw experiments show weaker soil uptake, with a mean  $v_d$  of  
470 (0.13±0.06) (2 SE, n=8) cm s<sup>-1</sup> for the net-uptake experiments (Table 1b) and

471 (0.06±0.03) (2 SE, n=9) cm s<sup>-1</sup> for the net-emission experiments (Table 2). In  
472 terms of the net H<sub>2</sub> flux  $F_n$ , this is (-26.5±4.8) (2 SE, n=12) nmol m<sup>-2</sup> s<sup>-1</sup> for  
473 Speuld experiments (Table 1a), (-13.6±8.6) (2 SE, n=8) nmol m<sup>-2</sup> s<sup>-1</sup> for Cabauw  
474 net-uptake experiments (Table 1b) and (49.5±29.8) (2 SE, n=9) nmol m<sup>-2</sup> s<sup>-1</sup> for  
475 Cabauw net-emission experiments (Table 2), indicating strong uptake, weaker  
476 uptake and strong emission of H<sub>2</sub>, respectively.

477

478

### 479 **3.3 Fractionation during soil uptake**

480

481 Soil uptake and soil emission have opposite effects on the isotopic composition  
482 of H<sub>2</sub> and can partly cancel each other. This will lead to additional uncertainty  
483 and we expect to obtain the most robust fractionation factor for soil uptake  
484 when the soil uptake is larger than the soil emission (Table 1a&b).

485

486 The resulting  $\alpha_{\text{soil}}$  for Speuld (Table 1a) varies from 0.913 to 0.955, with a mean  
487 value of 0.937±0.008 (2 SE, n=12). Error estimates for HH and HD mole  
488 fraction at time t and at equilibrium are considered for the final error estimates  
489 of  $\alpha_{\text{soil}}$  for each experiment.

490

491 Table 1b shows  $\alpha_{\text{soil}}$  of the Cabauw net-uptake experiments. It should be noted  
492 that the soil emitted  $\text{H}_2$  interferes much more with the fractionation during  
493 uptake in these Cabauw net-uptake experiments than for the Speuld experiments,  
494 which is illustrated by the consistent decrease in  $\delta\text{D}$  in the middle panel of Fig.  
495 6. The derived values for  $\alpha_{\text{soil}}$  vary from 0.911 to 1.019 with a mean value of  
496  $0.951 \pm 0.026$  (2 SE,  $n=8$ ) for these 8 selected Cabauw net-uptake experiments.  
497 Both the mean and the standard error are higher than for the Speuld experiments  
498 ( $0.937 \pm 0.008$ ), but the difference is not significant at the 0.1 confidence level.

499

500 To graphically illustrate the calculation of  $\alpha_{\text{soil}}$  with the mass balance model, we  
501 plot  $\ln \frac{c' - c'_{\text{e,app}}}{c'_1 - c'_{\text{e,app}}}$  versus  $\ln \frac{c - c_{\text{e,app}}}{c_1 - c_{\text{e,app}}}$  for all Speuld and Cabauw net-uptake  
502 experiments in Fig. 7. A linear fit is applied to all the data and the overall  $\alpha_{\text{soil,app}}$   
503 is found to be  $0.947 \pm 0.004$  (95% CI). Applying a correction factor is not  
504 straightforward now because this analysis combines the results from different  
505 experiments. If we use the average of  $\alpha_{\text{soil,true}} / \alpha_{\text{soil,app}}$  ratios (0.998) for all net-  
506 uptake experiments in Table 3 as the correction coefficient for this overall  
507  $\alpha_{\text{soil,app}}$ , the overall  $\alpha_{\text{soil}}$  is  $0.945 \pm 0.004$  (95% CI).

508

509 Fig. 8 shows  $\alpha_{\text{soil}}$  as a function of  $v_d$  for all Speuld experiments and Cabauw net-  
510 uptake experiments. The  $R^2$  value is nearly zero and the p-value is 0.53 for the  
511 linear regression of all experiments, so no significant correlation between  $\alpha_{\text{soil}}$

512 and  $v_d$  is found. Also, no significant correlation is found when considering the  
513 Speuld and Cabauw net-uptake experiments separately.

514

515

### 516 **3.4 Isotopic signature of H<sub>2</sub> emitted from soil**

517

518 As discussed in Section 2.4, the isotopic signature of H<sub>2</sub> emitted from the soil  
519 ( $\delta D_{\text{soil}}$ ) can be obtained from the mass balance model. In order to minimize the  
520 influence of soil uptake on the computed  $\delta D_{\text{soil}}$  and obtain the most robust result,  
521 we only consider the Cabauw experiments with strong soil emission and weak  
522 soil uptake ( $c_{e,\text{app}} > 1500$  ppb). In total, 9 Cabauw experiments are selected  
523 (Table 2) and a linear fit is applied to the plot of  $c'_{e,\text{app}} \ln \frac{c' - c'_{e,\text{app}}}{c'_1 - c'_{e,\text{app}}}$  versus  
524  $c_{e,\text{app}} \ln \frac{c - c_{e,\text{app}}}{c_1 - c_{e,\text{app}}}$  for each experiment (Fig. 9). It can be seen that the linear  
525 function fits the data very well for each experiment. The slope of the linear fit  
526 yields  $P'_{\text{app}}/P_{\text{app}}$ . This  $P'_{\text{app}}/P_{\text{app}}$  ratio is used to calculate  $\delta D_{\text{soil,app}}$  (Eq. (5)). After  
527 correcting for the flask sampling effects (see Appendix A), the corresponding  
528  $\delta D_{\text{soil}}$  values are shown in Table 2. The  $\delta D_{\text{soil}}$  value ranges from -629 ‰ to -  
529 451 ‰, with a mean value of  $(-530 \pm 40)$  ‰ (2 SE, n=9), which is very D-  
530 depleted, but still considerably enriched relative to the value around -700 ‰  
531 expected for thermodynamic equilibrium between H<sub>2</sub> and H<sub>2</sub>O (Bottinga, 1969).

532

533

## 534 **4. Discussion**

535

### 536 **4.1 Emission and uptake strength of H<sub>2</sub>**

537

538 The deposition velocity  $v_d$  is a measure of the strength of soil uptake. Both  
539 microbial removal and diffusion can affect  $v_d$ , and they can both be influenced  
540 by the temperature and moisture content of the soil (Ehhalt and Rohrer, 2013a;  
541 2013b). On average, the  $v_d$  obtained in this study is larger in the forest region  
542 (Table 1a) than in the grass/clover region (Table 1b and 2), in agreement with  
543 the conclusion from Ehhalt and Rohrer (2009).

544

545 The  $v_d$  of  $(0.06 \pm 0.03)$  cm s<sup>-1</sup> found in our Cabauw net-emission experiments  
546 (Table 2) is similar to those reported in Conrad and Seiler (1980) (0.07 cm s<sup>-1</sup>,  
547 both grass and clover) and Gerst and Quay (2001) (0.04 cm s<sup>-1</sup>, grass), while the  
548  $v_d$  of  $(0.13 \pm 0.06)$  cm s<sup>-1</sup> in Cabauw net-uptake experiments (Table 1b) is larger  
549 than those studies with similar soil cover but close to values of 0.12 to 0.14 cm  
550 s<sup>-1</sup> found in savanna soil (Conrad and Seiler, 1985). The stronger soil uptake in  
551 Speuld forest ( $(0.17 \pm 0.02)$  cm s<sup>-1</sup>) agrees well with the beech forest results (0.06  
552 to 0.22 cm s<sup>-1</sup>) in Förstel (1988) and Förstel and Führ (1992). However, other

553 studies at forest sites cited in Ehhalt and Rohrer (2009) showed lower  $v_d$  than  
554 our Speuld results. We note here that the  $v_d$  values reported in Conrad and Seiler  
555 (1980; 1985) were gross deposition velocities while those reported in Gerst and  
556 Quay (2001) were net deposition velocities. The specific method used to obtain  
557  $v_d$  was not documented in the other studies.  $v_d$  obtained from our experiments  
558 are gross deposition velocities.

559

560 The net uptake flux  $F_n$  in our Speuld experiments and Cabauw net-uptake  
561 experiments is much larger than those found in Smith-Downey et al. (2008).  
562 They found a  $F_n$  of about  $-8 \text{ nmol m}^{-2} \text{ s}^{-1}$  for the forest, desert, and marsh, which  
563 was similar to that for loess loamy soil in Schmitt et al. (2009). Our results are  
564 within the  $F_n$  range found in the mixed wood plains by Constant et al. (2008b)  
565 and the Harvard forest by Meredith (2012). Previously at our Cabauw site, Popa  
566 et al. (2011) obtained a  $F_n$  of only  $-3 \text{ nmol m}^{-2} \text{ s}^{-1}$  by using the radon tracer  
567 method. However, the Cabauw net-uptake experiments used for this evaluation  
568 were from selected places where uptake was strong, while the results in Popa et  
569 al. (2011) represented the overall uptake in the footprint of the Cabauw site,  
570 which is a much larger area (tens of  $\text{km}^2$ ).

571

572 Khdhiri et al. (2015) performed microbiological analyses on soil samples from  
573 the Cabauw and Speuld sites, in order to find the drivers of soil  $\text{H}_2$  uptake. They  
574 observed that the  $\text{H}_2$  uptake rate under standard incubation conditions was



575 significantly lower for the Cabauw soil samples than for the Speuld ones, which  
576 is consistent with our findings. The main factors that explained the differences  
577 were the relative abundance of high affinity H<sub>2</sub>-oxydizing bacteria and the soil  
578 carbon content, both lower on average for the Cabauw site.

579

580 The emission of H<sub>2</sub> from the soil is large for the Cabauw net-emission  
581 experiments, with  $F_n$  ranging from 13.7 to 150.2 nmol m<sup>-2</sup> s<sup>-1</sup> and a median  
582 value of 41.0 nmol m<sup>-2</sup> s<sup>-1</sup> (Table 2). One experiment, “CBW-28”, shows  
583 unusually high emission, with H<sub>2</sub> increasing to 3010 ppb within 30 minutes. In  
584 comparison, Conrad and Seiler (1980) found a  $F_n$  of 23-32 nmol m<sup>-2</sup> s<sup>-1</sup> for a  
585 clover field. Except for the experiments “CBW-28” and “CBW-31”, our  
586 Cabauw net-emission experiments are close to the  $F_n$  found by them. The  
587 variability in  $F_n$  could be attributed to different N<sub>2</sub> fixation flux in our  
588 experiments, which could be affected by both spatial density of N<sub>2</sub> fixation  
589 organisms and their N<sub>2</sub> fixation activities. The N<sub>2</sub> fixation activity could be  
590 regulated by various factors including temperature, moisture, light availability  
591 and carbon storage etc. (Belnap, 2001), which were not measured are therefore  
592 not discussed here.

593

594

## 595 **4.2 Fractionation during soil uptake**

596

597 Fractionation during soil uptake of  $H_2$  can happen during the diffusion into the  
598 soil and due to microbial removal within the soil. To further investigate the  
599 factors determining  $\alpha_{\text{soil}}$ , information about the soil cover is provided in Table  
600 1a&b. It is evident that no large differences exist between the Douglas fir,  
601 spruce and beech sites, i.e. the variability between sites is similar to the  
602 variability within sites. The small number of experiments impedes examining  
603 the possible small differences between sites. In order to investigate the diffusion  
604 effect, we removed the soil cover in experiments “SPU-8” and “SPU-12” at the  
605 same place of experiments “SPU-7” and “SPU-11”. The removal of leaves  
606 (“SPU-8”) and needles (“SPU-12”) increased  $\alpha_{\text{soil}}$  by  $\approx 0.014$ , thus towards  
607 smaller fractionation, which indicates that diffusion contributes to the  
608 fractionation. As  $v_d$  also increases when the soil cover is removed, faster  
609 deposition is associated with smaller fractionations in these experiments, which  
610 is similar to the results from Rice et al. (2011).

611

612 The  $\alpha_{\text{soil}}$  for the Cabauw net-uptake experiments is higher and more scattered  
613 than that for the Speuld experiments ( $0.951 \pm 0.026$  vs.  $0.937 \pm 0.008$ ). This could  
614 be caused by the interference of D-depleted  $H_2$  from the strong soil emission in  
615 Cabauw, which may not be perfectly captured via the mathematical models  
616 applied. As can be seen from the strong decline of  $\delta D$  with time in the middle  
617 panel of Fig. 6, though soil uptake of  $H_2$  dominates for the Cabauw net-uptake

618 experiments, soil production is still considerable. If part of the source signature  
619 is not taken into account properly and appears in  $\alpha_{\text{soil}}$ , then  $\alpha_{\text{soil}}$  will be larger,  
620 because soil production tends to decrease  $\delta D$  of  $H_2$ . This could explain why  $\alpha_{\text{soil}}$   
621 is even larger than 1 in “CBW-7”.

622

623 The overall  $\alpha_{\text{soil}}$  (0.945) obtained by plotting  $\ln \frac{c' - c'_{e,\text{app}}}{c'_1 - c'_{e,\text{app}}}$  versus  $\ln \frac{c - c_{e,\text{app}}}{c_1 - c_{e,\text{app}}}$  and  
624 applying the average correction factor for all the Speuld and Cabauw net-uptake  
625 experiments is similar to the results of  $0.943 \pm 0.024$  from Gerst and Quay (2001)  
626 and  $0.94 \pm 0.01$  from Rahn et al. (2002a). They suggested that the overall  $\alpha_{\text{soil}}$  is  
627 more accurate as it is less susceptible to outliers. We argue here that the average  
628  $\alpha_{\text{soil}}$  of all individual experiments in Speuld (0.937) and Cabauw (0.951) is  
629 representative for a spatially averaged fractionation factor for those sites and is  
630 useful for e.g. characterizing the phenomenon and comparing with other  
631 fractionation results. If all experiments are included in one fit, their weight for  
632 determining the slopes depends on how much  $H_2$  has been removed, so  
633 experiments with a lower  $c_{e,\text{app}}$  have a larger weight than experiments with a  
634 higher  $c_{e,\text{app}}$  (i.e. experiments with a higher  $v_d$  have a larger weight than  
635 experiments with a lower  $v_d$ ). The fractionation factor obtained by fitting all  
636 data together is therefore representative for a flux weighted average, which is  
637 the relevant number for the global atmospheric isotope budget.

638

### 639 **4.3 Relationship between $\alpha_{\text{soil}}$ and $v_d$**

640

641 Rice et al. (2011) proposed a significant positive correlation between  $\alpha$  and  
642 deposition velocity  $v_d$  in their soil uptake experiments. Fig. 8 shows that no  
643 significant correlation between  $\alpha_{\text{soil}}$  and  $v_d$  is found when considering all Speuld  
644 and Cabauw net-uptake experiments. The uptake rate is much stronger in the  
645 Speuld experiments ( $v_d \approx 0.17 \text{ cm s}^{-1}$ ) than in the study of Rice et al. (2011) ( $v_d$   
646  $\approx 0.04 \text{ cm s}^{-1}$ ), but the  $\alpha_{\text{soil}}$  is virtually identical (0.937 *versus* 0.934). Therefore,  
647 when the results from both studies are combined, the correlation reported in  
648 Rice et al. (2011) between  $\alpha_{\text{soil}}$  and  $v_d$  disappears. We suggest that a positive  
649 correlation between  $\alpha_{\text{soil}}$  and  $v_d$  may exist for a specific site where microbial  
650 species are similar. This was suggested from the simultaneous increase of both  
651  $\alpha_{\text{soil}}$  and  $v_d$  in two experiments (“SPU-8” and “SPU-12”), when soil cover was  
652 removed at the same sampling location, as mentioned in Section 4.2.

653

654 We conclude that there is certainly not one single correlation between  $\alpha_{\text{soil}}$  and  
655  $v_d$  that holds globally and the soil type might play an important role.  
656 Measurements at more sites may be needed to positively confirm whether local  
657 positive correlations between  $\alpha_{\text{soil}}$  and  $v_d$  are common.

658

659

#### 660 **4.4 $\delta D$ of $H_2$ emitted from the soil**

661

662 The present study is the first field study to report  $\delta D$  of  $H_2$  emitted from soils.  
663 The  $\delta D_{\text{soil}}$  values (-629 ‰ to -451 ‰) shown in Table 2 are less depleted than  
664 the  $H_2$  in isotopic equilibrium with water ( $\approx -700$  ‰). Previous observations  
665 from environmental  $H_2$  production yielded a  $\delta D$  of -628 ‰ for two seawater  
666 samples (Rice et al., 2010), -778 ‰ for a termite headspace sample and -690 ‰  
667 for two headspace samples from a eutrophic water pond (Rahn et al., 2002b).  
668 Kawagucci et al. (2015) proposed that microbiological  $H_2$  consumption and  
669 production could destroy the thermal isotopic equilibrium between  $H_2$  and  $H_2O$   
670 in low-temperature hydrothermal fluids. Luo et al. (1991) and Walter et al.  
671 (2012) found fractionation factors of 0.448, 0.401 and 0.363 for  $H_2$  generated  
672 from water by different  $N_2$ -fixing bacteria in the laboratory.

673

674 In order to compare our  $\delta D_{\text{soil}}$  with the fractionation factors between  $H_2$  and  
675  $H_2O$  found by Luo et al. (1991) and Walter et al. (2012), we converted their  
676 fractionation factors to  $\delta D(H_2)$  by assuming the  $\delta D(H_2O)$  to be the same as that  
677 of global rainwater (-37.8 ‰, Hoffmann et al., 1998). This results in  $\delta D(H_2)$   
678 values of -651 ‰ to -569 ‰ for their  $N_2$ -fixing bacteria. Although the ranges  
679 are considerable, it appears that the mean  $\delta D_{\text{soil}}$  (-530 ‰) obtained in our field

680 study is even higher than what was found for nitrogenase-derived H<sub>2</sub> in  
681 laboratory experiments.

682

683 It is known that H<sub>2</sub> produced by biogenic N<sub>2</sub> fixation can be largely recycled  
684 within the soil before entering the atmosphere (Evans et al., 1987; Conrad and  
685 Seiler, 1979; 1980). If this uptake process within the soil tends to increase the  
686  $\delta D$  of the remaining H<sub>2</sub>, as the soil uptake process for atmospheric H<sub>2</sub> does, then  
687 the H<sub>2</sub> entering the atmosphere will be less D-depleted than pure biogenic H<sub>2</sub>.  
688 However, if the fractionation factor of removal in the soil is similar to that  
689 determined from the net-uptake experiments ( $\approx 0.94$ ), a large fraction ( $f_{in}$ ) of H<sub>2</sub>  
690 needs to be removed in the soil before release to explain the D-enriched  $\delta D_{soil}$   
691 compared to the values reported in the literature. The fraction  $f_{in}$  could in  
692 principle be estimated from the Rayleigh equation:

$$(1 - f_{in})^{\alpha_{in}-1} = \frac{\delta D_{soil} + 1}{\delta D_0 + 1}$$

693 where  $\alpha_{in}$  is the fractionation constant of H<sub>2</sub> within soil,  $\delta D_0$  is the  $\delta D$  value of  
694 initial H<sub>2</sub> produced by N<sub>2</sub>-fixers, and  $\delta D_{soil}$  is the  $\delta D$  value of remaining H<sub>2</sub>  
695 emitted from soil that is measured in our experiments. By assuming  $\alpha_{in}=0.945$   
696 (overall fractionation factor as determined in our deposition experiments),  
697  $\delta D_{soil}=-530 \text{ ‰}$  (averaged  $\delta D_{soil}$  of Cabauw net-emission experiments) and  $\delta D_0=-$   
698  $611 \text{ ‰}$  (averaged of  $\delta D(H_2)$  derived from laboratory experiments in Luo et al.  
699 (1991) and Walter et al. (2012)), we would obtain  $f_{in}=0.97$ . That is, 97% of H<sub>2</sub>

700 produced by  $N_2$  fixation would be removed within soil before entering  
701 atmosphere. This is higher than the estimate from Conrad and Seiler (1979),  
702 which was from 30% to 90%. It should be noted that the estimation of  $f_{in}$  is very  
703 uncertain due to the lack of information about  $\alpha_{in}$  and  $\delta D_0$ . By using the lower  
704 limit of  $\alpha_{in}$  (0.911) in our experiment and the upper limit of  $\delta D_0$  (-569 ‰) in  
705 Luo et al. (1991) and Walter et al. (2012), we calculate a lower limit of  $f_{in}$  to be  
706 0.62. The upper limit of  $f_{in}$  is 1.00 when  $\alpha_{in}$  approaches 1. For these calculations  
707 we have used a  $\delta D_{soil}$  of -530 ‰, but it varies from -629 ‰ to -451 ‰ in our  
708 experiments. We cannot rule out cases with  $\delta D_{soil} = \delta D_0$ , which yields a  $f_{in}$  of 0.

709

710 The deuterium enrichment in the emitted  $H_2$ , compared to the value expected in  
711 isotopic equilibrium with water, could also be caused by different fractionations  
712 induced by different enzymes and/or a potentially enriched deuterium content of  
713 the substrate water available for  $H_2$  production in Cabauw.  $H_2$  is generated from  
714 the reduction of hydrogen ions ( $H^+$  or  $D^+$ ) in intracellular water (Yang et al.,  
715 2012). It was found that the isotopic composition of intracellular water can be  
716 different from that of extracellular water due to metabolic processing (Kreuzer-  
717 Martin et al., 2006). Due to the differences in H-bonding and hydrogen ion  
718 transport, the fractionation may be different for different microbe species, which  
719 could result in different isotopic signatures of the produced  $H_2$ . Measurements  
720 of the isotopic composition of produced  $H_2$  may be a tool to investigate such  
721 effects.

722

723 Finally, we note that if our Cabauw net-emission experiments are analyzed with  
724 a simple Keeling plot approach (i.e. without considering uptake), the y axis  
725 intercept is -703 ‰. We know from the temporal evolution of H<sub>2</sub>, HD and δD  
726 that this model is not adequate and that uptake was significant in our  
727 experiments, so a simple Keeling plot analysis can be misleading if uptake is  
728 not considered.

729

730

## 731 **5. Conclusions**

732

733 This study investigated the isotope effects associated with the production and  
734 uptake of atmospheric H<sub>2</sub> by soil. Our aim was to quantify the fractionation  
735 factor  $\alpha_{\text{soil}}$  for H<sub>2</sub> deposition and the isotopic signature of H<sub>2</sub> emitted from the  
736 soil ( $\delta D_{\text{soil}}$ ) from experiments carried out at Speuld and Cabauw.

737

738 The experiments covered a wide range of conditions from situations with very  
739 strong net H<sub>2</sub> uptake to situations with very strong net H<sub>2</sub> emission. The  
740 superposition of deposition and production made the analysis with simple  
741 models like Rayleigh plot and Keeling plot impossible. Therefore, the mass  
742 balance model suggested by Rice et al. (2011) was used for evaluation.



743

744 The deposition velocity  $v_d$  was largest in the Speuld experiments ((0.17±0.02)  
745 cm s<sup>-1</sup>) where also the strongest net soil uptake occurred, followed by the  
746 Cabauw net-uptake experiments ((0.13±0.06) cm s<sup>-1</sup>) and Cabauw net-emission  
747 experiments ((0.06±0.03) cm s<sup>-1</sup>). The net H<sub>2</sub> flux  $F_n$  was (-26.5±4.8) nmol m<sup>-2</sup>  
748 s<sup>-1</sup> for Speuld experiments, (-13.6±8.6) nmol m<sup>-2</sup> s<sup>-1</sup> for Cabauw net-uptake  
749 experiments and (49.5±29.8) nmol m<sup>-2</sup> s<sup>-1</sup> for Cabauw net-emission  
750 experiments.

751

752 The mean fractionation factors  $\alpha_{\text{soil}}$  are 0.937±0.008 for the Speuld forest soil  
753 experiments and 0.951±0.026 for the Cabauw grassland experiments, which are  
754 representative for a spatial average and useful for comparisons with other  
755 fractionation studies. The Cabauw results may be affected by the relatively  
756 strong concomitant soil emissions. The overall  $\alpha_{\text{soil}}$  by considering all net-  
757 uptake experiments is 0.945±0.004, which is representative for a flux weighted  
758 average and useful for global isotope budget estimates. The fractionation factors  
759 found in this work are in good agreement with previous studies.

760

761 No significant correlation between  $\alpha_{\text{soil}}$  and deposition velocity  $v_d$  was found  
762 while considering all of our experiments. The  $v_d$  were overall much larger in our  
763 study than those in Rice et al. (2011) and we obtained similar values for  $\alpha_{\text{soil}}$ .  
764 This demonstrates that the positive correlation that was found previously does

765 not hold globally. From two of our Speuld experiments,  $\alpha_{\text{soil}}$  increased after the  
766 removal of leaves or needles above the soil. This indicates that there may be a  
767 fractionation associated with diffusion through the surface layer of leaves or  
768 needles during soil uptake, but more experiments are required to confirm this.

769

770 The isotopic analysis clearly showed that the net uptake was always a  
771 superposition of a larger gross uptake and a gross emission flux. In Cabauw, the  
772 emission strength was very large at locations where clover was present. Using a  
773 simple mass balance approach, the isotopic composition of the emitted  $\text{H}_2$  was  
774 determined to be  $(-530 \pm 40) \text{‰}$ , which is significantly higher than the value  
775 expected for  $\text{H}_2\text{O} - \text{H}_2$  isotope equilibrium. Although limited, other published  
776 data on  $\text{H}_2$  produced biologically via nitrogenase show also a tendency to more  
777 enriched values. An additional isotope enrichment in our field soil study could  
778 originate from fractionation during the recycling of  $\text{H}_2$  within the soil before it  
779 enters the atmosphere.

780

## 781 **Appendix A**

782

### 783 **A1. Flask sampling model**

784

785 A mathematical model is used to simulate the sampling and to correct for the  
786 effects of the flask sampling method on the values of uptake rate constant ( $k$ ),  
787 production rate ( $P$ ), fractionation factor ( $\alpha_{\text{soil}}$ ) and isotopic signature of  $\text{H}_2$   
788 produced from soil ( $\delta\text{D}_{\text{soil}}$ ). We start with a pair of known (*true*) uptake and  
789 production rates and simulate the evolution of the mole fractions of  $\text{H}_2$  and HD  
790 in the flasks and chamber. From the modeled mole fractions we calculate the  
791 *apparent* uptake and production rates and derive the correction needed to obtain  
792 the *true* uptake and production rates from measurement of the *apparent* rates in  
793 actual experiments.

794

#### 795 **A1.1 Mathematical description of the flask sampling model**

796

797 The sampling setup is shown in Fig. 2 of the main paper. After 10 minutes of  
798 flushing, the chamber and the flasks contain ambient air with the prevailing  $\text{H}_2$   
799 and HD mole fractions. In the following we denote  $c_1(t)$ ,  $c_2(t)$ ,  $c_3(t)$ ,  $c_4(t)$  and  
800  $c_0(t)$  the  $\text{H}_2$  mole fractions for the first, second, third, fourth flask and the  
801 chamber, respectively. The moment when the first flask and the chamber lid are

802 closed is considered the starting time of the experiment ( $t=0$ ). From this point  
803 on, only the chamber, the second, third and fourth flask are connected, and the  
804 initial  $H_2$  mole fraction inside them is  $c_0(0) = c_2(0) = c_3(0) = c_4(0) = c_1$ . We start  
805 a simulation with an input uptake rate constant ( $k_{\text{true}}$ ) and an input production  
806 rate ( $P_{\text{true}}$ ). The simulation of the flask sampling is based on Eqs. (A1)-(A4)  
807 shown below.

808

809 Assuming that the air in each flask and in the chamber is well-mixed during the  
810 entire sampling process, the time evolution for the second flask  $c_2(t)$ , the third  
811 flask  $c_3(t)$ , the fourth flask  $c_4(t)$  and the chamber  $c_0(t)$  in the first 10 minutes after  
812 starting the experiment can be expressed as:

813

$$\frac{dc_2(t)}{dt} = \frac{f}{V} c_0(t) - \frac{f}{V} c_2(t) \quad (\text{A1})$$

814

$$\frac{dc_3(t)}{dt} = \frac{f}{V} c_2(t) - \frac{f}{V} c_3(t) \quad (\text{A2})$$

815

$$\frac{dc_4(t)}{dt} = \frac{f}{V} c_3(t) - \frac{f}{V} c_4(t) \quad (\text{A3})$$

816

$$\frac{dc_0(t)}{dt} = \frac{f}{V'} c_4(t) - \frac{f}{V'} c_0(t) + (P_{\text{true}} - k_{\text{true}} c_0(t)) \quad (\text{A4})$$

817

818 where  $V$  and  $V'$  are the air volumes of the flask and chamber, and  $f$  is the flow  
819 rate. These differential equations are solved using the Matlab ODE solvers at  
820 time steps of 0.01 min. The input parameters are  $c_0(0)$ ,  $P_{\text{true}}$ ,  $k_{\text{true}}$ ,  $V$ ,  $V'$  and  $f$ .  
821 For each time step the solvers calculate the hydrogen flux into and out of the  
822 chamber and each flask, as well as the new mole fractions there.

823

824 After 10 minutes, the second flask is closed and now contains air with mole  
825 fraction  $c_2 = c_2(10 \text{ min})$ . From this point on, only the chamber, the third and the  
826 fourth flask are connected, and the time evolution of the mole fractions can be  
827 expressed as:

828

$$\frac{dc_3(t)}{dt} = \frac{f}{V} c_0(t) - \frac{f}{V} c_3(t) \quad (\text{A5})$$

829

$$\frac{dc_4(t)}{dt} = \frac{f}{V} c_3(t) - \frac{f}{V} c_4(t) \quad (\text{A6})$$

830

$$\frac{dc_0(t)}{dt} = \frac{f}{V'} c_4(t) - \frac{f}{V'} c_0(t) + (P_{\text{true}} - k_{\text{true}} c_0(t)) \quad (\text{A7})$$

831

832 After another 10 minutes of sampling, the third flask is closed  $c_3 = c_3(20 \text{ min})$ ,  
833 and only the chamber and the fourth flask are connected. Then, the time  
834 evolution for the fourth flask and the chamber can be expressed as:

835

$$\frac{dc_4(t)}{dt} = \frac{f}{V} c_0(t) - \frac{f}{V} c_4(t) \quad (\text{A8})$$

836

$$\frac{dc_0(t)}{dt} = \frac{f}{V'} c_4(t) - \frac{f}{V'} c_0(t) + (P_{\text{true}} - k_{\text{true}} c_0(t)) \quad (\text{A9})$$

837

838 The H<sub>2</sub> mole fraction inside the chamber and the fourth flask at time t=30  
839 minutes is c<sub>0</sub>(30) and c<sub>4</sub>(30).

840

841 In the end, a set of four flasks with mole fractions c<sub>1</sub>(0), c<sub>2</sub>(10 min), c<sub>3</sub>(20 min)  
842 and c<sub>4</sub>(30 min) is obtained. By fitting this set of four data points with an  
843 exponential function  $c = ae^{-k_{\text{app}}t} + c_{\text{e,app}}$  (see Eq. (2) in the main paper), we  
844 can obtain the *apparent* soil uptake rate constant ( $k_{\text{app}}$ ) and equilibrium  
845 concentration ( $c_{\text{e,app}}$ ) and further calculate *apparent* production rate  
846 ( $P_{\text{app}} = k_{\text{app}} c_{\text{e,app}}$ ). These apparent rates  $k_{\text{app}}$  and  $P_{\text{app}}$  are different from the assumed  
847 *true* rates  $k_{\text{true}}$  and  $P_{\text{true}}$ . The flask sampling model enables us to establish a  
848 relation between  $k_{\text{app}}$  and  $P_{\text{app}}$  and  $k_{\text{true}}$  and  $P_{\text{true}}$ , so that  $k_{\text{true}}$  and  $P_{\text{true}}$  can be  
849 derived from  $k_{\text{app}}$  and  $P_{\text{app}}$  in actual experiments, where the true values are  
850 unknown. To accomplish this, simulations are carried out with a wide range of  
851 values for  $k_{\text{true}}$  and  $P_{\text{true}}$ , and a corresponding dataset of  $k_{\text{app}}$  and  $P_{\text{app}}$  is generated.

852 Similarly, we use a new set of input uptake rate constant  $k'_{\text{true}}$  and production  
853 rate  $P'_{\text{true}}$  for HD, and generate a corresponding dataset of  $k'_{\text{app}}$  and  $P'_{\text{app}}$ .

854

## 855 **A1.2 The correction coefficients for $k$ and $P$**

856

857 Here we discuss an example of the relationship between  $k_{\text{true}}$  and  $k_{\text{app}}$  for the  
858 setup used in some Cabauw experiments ( $V=22.8$  L,  $f=2$  L  $\text{min}^{-1}$  and  $\Delta t=10$   
859 min). The pressure inside the flasks is 200 kPa and the pressure inside the  
860 chamber is 100 kPa. The relationship between  $k_{\text{true}}/k_{\text{app}}$  and  $k_{\text{app}}$  is shown in Fig.  
861 10a. The ratio  $k_{\text{true}}/k_{\text{app}}$  varies between 1.45 to 1.61 for our  $k_{\text{app}}$  range of 0.04 to  
862 0.30  $\text{min}^{-1}$ . This relationship does not depend on  $P_{\text{true}}$  (with  $P_{\text{true}}$  varying from 50  
863 to 650 ppb  $\text{min}^{-1}$ ). An additional uncertainty can arise from incorrect timing of  
864 the flask sampling, but sampling times should be correct within few seconds,  
865 which may lead to an additional uncertainty of below 1%. The uncertainty of  
866 the flow rate obtained from the rotameter due to variations in ambient pressure  
867 and temperature that were not recorded is less than 4%, and the effect on the  
868 ratio  $k_{\text{true}}/k_{\text{app}}$  ratio is below 1%. We can retrieve  $k_{\text{true}}$  by multiplying  $k_{\text{app}}$  with the  
869 modeled value of  $k_{\text{true}}/k_{\text{app}}$  for each experiment. The ratio  $k_{\text{true}}/k_{\text{app}}$  for each  
870 experiment is shown in Table 3. It depends on experimental setup and  $k_{\text{app}}$  of  
871 each experiment, with a range of 1.177 to 1.589.

872

873 After retrieving  $k_{\text{true}}$  from  $k_{\text{app}}$ , we investigate the relationship between  $P_{\text{true}}/P_{\text{app}}$   
874 and  $P_{\text{app}}$  for a fixed value of  $k_{\text{true}}$  (Fig. 10b). The ratio  $P_{\text{true}}/P_{\text{app}}$  depends slightly  
875 on  $P_{\text{app}}$  and  $k_{\text{true}}$ , ranging from 1.40 to 1.59 for a wide  $P_{\text{app}}$  range of 30 to 450  
876 ppb  $\text{min}^{-1}$  and a wide  $k_{\text{true}}$  range of 0.05 to 0.45  $\text{min}^{-1}$ . As for the correction of  $k$ ,  
877 uncertainties arising from incorrect timing of the flask sampling and from  
878 pressure and temperature variations and their effect on the flow rate lead to  
879 additional uncertainties of  $P_{\text{true}}/P_{\text{app}}$  ratio below 1%, which are not considered.  
880 We can retrieve  $P_{\text{true}}$  by multiplying  $P_{\text{app}}$  with  $P_{\text{true}}/P_{\text{app}}$  for each experiment after  
881 having determined  $k_{\text{true}}$  from  $k_{\text{app}}$ . The ratio  $P_{\text{true}}/P_{\text{app}}$  for each experiment is  
882 shown in Table 3 and depends on the experimental setup,  $P_{\text{app}}$  and  $k_{\text{app}}$  of each  
883 experiment. It ranges from 1.152 to 2.759 for most experiments, with an  
884 exception of 7.472 for experiment SPU-2 where a very small  $P_{\text{app}}$  of 0.67 ppb  
885  $\text{min}^{-1}$  is found. Although the ratio  $P_{\text{true}}/P_{\text{app}}$  of experiment SPU-2 is high,  $P_{\text{true}}$  of  
886 SPU-2 is still smaller than the rest of the experiments.  $P_{\text{true}}/P_{\text{app}}$  ratios for  
887 experiments SPU-10 and SPU-11 are null because these two experiments show  
888 a  $P_{\text{app}}$  of zero.

889

### 890 **A1.3 The correction coefficients for $\alpha_{\text{soil}}$ and $\delta D_{\text{soil}}$**

891

892 In our experiments, the uncertainties of  $k_{\text{app}}$  and  $k'_{\text{app}}$  derived from exponential  
893 fits to the time evolution of HH and HD are rather large, which results in a large  
894 scatter of  $\alpha_{\text{soil,app}}$  if  $\alpha_{\text{soil,app}}$  is calculated directly as  $k'_{\text{app}}/k_{\text{app}}$ . Thus, we obtained



895  $\alpha_{\text{soil,app}}$  by plotting  $\ln \frac{c'_1 - c'_{e,\text{app}}}{c'_1 - c'_{e,\text{app}}}$  versus  $\ln \frac{c - c_{e,\text{app}}}{c_1 - c_{e,\text{app}}}$  (Fig. 7) for each experiment

896 which yields a smaller scatter for  $\alpha_{\text{soil,app}}$ .

897

898 Correction coefficients to convert  $\alpha_{\text{soil,app}}$  to  $\alpha_{\text{soil,true}}$  are obtained using the flask

899 sampling model by comparing  $\alpha_{\text{soil,true}}$  used as input for the model run to  $\alpha_{\text{soil,app}}$

900 derived from the plot of  $\ln \frac{c'_1 - c'_{e,\text{app}}}{c'_1 - c'_{e,\text{app}}}$  versus  $\ln \frac{c - c_{e,\text{app}}}{c_1 - c_{e,\text{app}}}$  of the output values, like

901 in the experiments. Fig. 10c shows  $\alpha_{\text{soil,true}}/\alpha_{\text{soil,app}}$  as a function of  $\alpha_{\text{soil,app}}$  for a

902 wide  $\delta D_{\text{soil,true}}$  range of -750‰ to -250‰ with the sampling setup described

903 above ( $V'=22.8$  L,  $f=2$  L  $\text{min}^{-1}$  and  $\Delta t=10$  min) for  $k_{\text{true}}=0.25$   $\text{min}^{-1}$  and  $P_{\text{true}}=50$

904 ppb  $\text{min}^{-1}$ . In this case the correction factor  $\alpha_{\text{soil,true}}/\alpha_{\text{soil,app}}$  varies from 0.98 to

905 1.00 for a  $\alpha_{\text{soil,app}}$  range of 0.90 to 1.00, and it does not depend on  $\delta D_{\text{soil,true}}$ . Thus,

906 after retrieving  $k_{\text{true}}$  and  $P_{\text{true}}$  as described in Section A1.2, we can retrieve  $\alpha_{\text{soil,true}}$

907 from  $\alpha_{\text{soil,app}}$  for each experiment. The correction factors range from 0.984 to

908 1.007, depending on the experimental setup and  $\alpha_{\text{soil,app}}$  of each experiment

909 (Table 3).

910

911 Similarly, in our experiments, the uncertainties of  $P_{\text{app}}$  and  $P'_{\text{app}}$  derived from

912 exponential fits of time evolution of HH and HD are large, which results in a

913 large scatter of  $\delta D_{\text{soil,app}}$  if  $\delta D_{\text{soil,app}}$  is calculated directly from these  $P'_{\text{app}}$  and  $P_{\text{app}}$ .

914 We therefore obtained the ratio  $P'_{\text{app}}/P_{\text{app}}$  by plotting  $c'_{e,\text{app}} \ln \frac{c'_1 - c'_{e,\text{app}}}{c'_1 - c'_{e,\text{app}}}$  versus

915  $c_{e,app} \ln \frac{c-c_{e,app}}{c_1-c_{e,app}}$  (Fig. 9) and calculated  $\delta D_{soil,app}$  from Eq. (4). This yielded  
916 smaller scatter for  $\delta D_{soil,app}$ . After retrieving  $k_{true}$ ,  $P_{true}$  and  $\alpha_{soil,true}$  as described  
917 above, we used the flask sampling model again to derived correction factors by  
918 comparing  $\delta D_{soil,true}$  used as model input with  $\delta D_{soil,app}$  obtained from  
919  $c'_{e,app} \ln \frac{c'-c'_{e,app}}{c'_1-c'_{e,app}}$  versus  $c_{e,app} \ln \frac{c-c_{e,app}}{c_1-c_{e,app}}$  of the model output, and retrieve  
920  $\delta D_{soil,true}$  from  $\delta D_{soil,app}$  for each experiment. Fig. 10d shows  
921  $(\delta D_{soil,true}+1)/(\delta D_{soil,app}+1)$  as a function of  $(\delta D_{soil,app}+1)$  for a  $\alpha_{soil,true}$  range of 0.90  
922 to 1.00 with the sampling setup described above ( $V'=22.8$  L,  $f=2$  L  $\text{min}^{-1}$  and  
923  $\Delta t=10$  min) for  $k_{true}=0.25$   $\text{min}^{-1}$  and  $P_{true}=50$  ppb  $\text{min}^{-1}$ . The ratio  
924  $(\delta D_{soil,true}+1)/(\delta D_{soil,app}+1)$  changes from 0.99 to 1.05 for a wide  $(\delta D_{soil,app}+1)$   
925 range of 0.25 to 0.65. It can be seen that the  $(\delta D_{soil,true}+1)/(\delta D_{soil,app}+1)$  ratio  
926 depends slightly on  $\alpha_{soil,true}$  at a fixed  $(\delta D_{soil,app}+1)$ , with a maximum difference  
927 of about 1% for a  $\alpha_{soil,true}$  range of 0.90 to 1.00. The ratio  
928  $(\delta D_{soil,true}+1)/(\delta D_{soil,app}+1)$  for each net-emission experiment is shown in Table 3,  
929 ranging from 1.007 to 1.048. The largest difference between  $\delta D_{soil,true}$  and  
930  $\delta D_{soil,app}$  is 21‰ for CBW-8. The mean  $\delta D_{true}$  and  $\delta D_{app}$  for these net emission  
931 experiments are -530‰ and -538‰, respectively.

932

933 In conclusion, the effect of the flask sampling process is relatively small for  $\alpha_{soil}$   
934 and  $\delta D_{soil}$ , but considerable for the uptake rate constants  $k$  and  $k'$  and emission  
935 rates  $P$  and  $P'$ . The flask sampling model allows to derive corresponding

936 corrections that have been applied to correct for the bias introduced by the flask  
937 sampling system.

938

939

#### 940 **Acknowledgements**

941

942 We are grateful to C. Van der Veen, M. Bolder and H. Snellen for their help on  
943 maintaining the GC-IRMS system and set-up of the sampling. We are also  
944 grateful to Jan Kaiser for giving valuable comments on the flask sampling  
945 model. This work was supported by the Dutch National Science foundation  
946 NWO as part of the NWO-ACTS Sustainable Hydrogen (H<sub>2</sub>) project  
947 2007/00566/ACTS, grant numbers 053.61.026 and 053.61.126.

948

949

950

951

952

953

954

955

956

957

958 **References**

959

960 Batenburg, A. M., Walter, S., Pieterse, G., Levin, I., Schmidt, M., Jordan, A.,  
961 Hammer, S., Yver, C., and Röckmann, T.: Temporal and spatial variability of the  
962 stable isotopic composition of atmospheric molecular hydrogen: observations at six  
963 EUROHYDROS stations, *Atmos. Chem. Phys.*, 11, 6985–6999, doi:10.5194/acp-11-  
964 6985-2011, 2011.

965

966 Beljaars, A. C. M. and Bosveld, F. C.: Cabauw data for the validation of land surface  
967 parameterization schemes, *J. Climate*, 10, 1172-1193, doi: 10.1175/1520-  
968 0442(1997)010<1172:CDFTVO>2.0.CO;2, 1997.

969

970 Belnap, J.: Factors influencing nitrogen fixation and nitrogen release in biological soil  
971 crusts, Springer-Verlag, Berlin Heidelberg, 241–261, 2001.

972

973 Bottinga, Y.: Calculated fractionation factors for carbon and hydrogen isotope  
974 exchange in the system calcite-carbon dioxide-graphite-methane-hydrogen-water  
975 vapour, *Geochim. Cosmochim. Ac.*, 33, 49–64, doi:10.1016/0016-7037(69)90092-1,  
976 1969.

977

978 Conrad, R.: Compensation concentration as critical variable for regulating the flux of  
979 trace gases between soil and atmosphere, *Biogeochemistry*, 27, 155–170,  
980 doi:10.1007/BF00000582, 1994.

981

982 Conrad, R. and Seiler W.: Field measurements of hydrogen evolution by nitrogen-  
983 fixing legumes, *Soil Biol. Biochem.*, 11, 689-690, doi: 10.1016/0038-0717(79)90041-  
984 5, 1979.

985

986 Conrad, R. and Seiler, W.: Contribution of hydrogen production by biological  
987 nitrogen fixation to the global hydrogen budget, *J. Geophys. Res.*, 85, 5493-5498, doi:  
988 10.1029/JC085iC10p05493, 1980.

989

990 Conrad, R. and Seiler, W.: Decomposition Of atmospheric hydrogen by soil  
991 microorganisms and soil enzymes, *Soil Biol. Biochem.*, 13, 43–49, doi: 10.1016/0038-  
992 0717(81)90101-2, 1981.

993

994 Conrad, R. and Seiler, W.: Influence of temperature, moisture, and organic carbon on  
995 the flux of H<sub>2</sub> and CO between soil and atmosphere: field studies in subtropical  
996 regions, *J. Geophys. Res.*, 90, 5699–5709, doi: 10.1029/JD090iD03p05699, 1985.

997

998 Conrad, R., Weber, M., and Seiler, W.: Kinetics and electron transport of soil  
999 hydrogenases catalyzing the oxidation of atmospheric hydrogen, *Soil Biol. and*  
1000 *Biochem.*, 15, 167-173, doi: 10.1016/0038-0717(83)90098-6, 1983.

1001

1002 Constant, P., Poissant, L., and Villemur, R.: Isolation of *Streptomyces* sp. PCB7, the  
1003 first microorganism demonstrating high-affinity uptake of tropospheric H<sub>2</sub>, *ISME J.*, 2,  
1004 1066-1076, doi: 10.1038/ismej.2008.59, 2008a.

1005

1006 Constant, P., Poissant, L., and Villemur, R.: Annual hydrogen, carbon monoxide and  
1007 carbon dioxide concentrations and surface to air exchanges in a rural area (Québec,  
1008 Canada), *Atmos. Environ.*, 42, 5090-5100, doi: 10.1016/j.atmosenv.2008.02.021,  
1009 2008b.

1010

1011 Constant, P., Chowdhury, S. P., Pratscher, J., and Conrad, R.: *Streptomyces*  
1012 contributing to atmospheric molecular hydrogen soil uptake are widespread and  
1013 encode a putative high-affinity [NiFe]-hydrogenase, *Environ. Microbiol.*, 12, 821-829,  
1014 doi:10.1111/j.1462-2920.2009.02130.x, 2010.

1015

1016 Constant, P., Chowdhury, S. P., Hesse, L., and Conrad, R.: Co-localization of  
1017 atmospheric H<sub>2</sub> oxidation activity and high affinity H<sub>2</sub>-oxidizing bacteria in non-  
1018 axenic soil and sterile soil amended with *Streptomyces* sp. PCB7. *Soil Biol.*  
1019 *Biochem.*, 43, 1888-1893, doi: 10.1016/j.soilbio.2011.05.009, 2011.

1020

1021 De Wit, J. C., Van der Straten, C. M., and Mook, W. G.: Determination of the  
1022 absolute isotopic ratio of V-SMOW and SLAP, *Geostandards Newsletter*, 4, 33-36,  
1023 doi:10.1111/j.1751-908X.1980.tb00270.x, 1980.

1024

1025 Ehhalt, D. H. and Rohrer, F.: The tropospheric cycle of H<sub>2</sub>: a critical review, *Tellus B*,  
1026 61(3), 500–535, doi:10.1111/j.1600-0889.2009.00416.x, 2009.

1027

1028 Ehhalt, D. H. and Rohrer, F.: The dependence of soil H<sub>2</sub> uptake on temperature and  
1029 moisture: a reanalysis of laboratory data, *Tellus B*, 63(5), 1040-1051,  
1030 doi: 10.1111/j.1600-0889.2011.00581.x, 2011.

1031

1032 Ehhalt, D. H. and Rohrer, F.: Deposition velocity of H<sub>2</sub>: a new algorithm for its  
1033 dependence on soil moisture and temperature, *Tellus B*, 65, 19904  
1034 doi:10.3402/tellusb.v65i0.19904, 2013a.

1035

1036 Ehhalt, D. H. and Rohrer, F.: Dry deposition of molecular hydrogen in the presence of  
1037 H<sub>2</sub> production, *Tellus B*, 65, 20620, doi:10.3402/tellusb.v65i0.20620, 2013b.

1038

1039 Evans, H. J., Harker, A. R., Papen, H., Russell, S. A., Hanus, F. J., and Zuber, M.:  
1040 Physiology, biochemistry, and genetics of the uptake hydrogenase in rhizobia, *Annu.*  
1041 *Rev. Microbiol.*, 41(1), 335-361, 1987.

1042

1043 Gerst, S. and Quay, P.: The deuterium content of atmospheric molecular hydrogen:  
1044 Method and initial measurements, *J. Geophys. Res.*, 105, 26433–26445,  
1045 doi:10.1029/2000JD900387, 2000.

1046

1047 Förstel, H.: HT to HTO conversion in the soil and subsequent tritium pathway: field  
1048 release data and laboratory experiments, *Fusion Tech.*, **14**, 1241–1246, 1988.

1049

1050 Förstel, H. and Führ, F.: Trockene Deposition von Tritium in den Boden, Annual  
1051 Report, Forschungszentrum Jülich, Jülich, 45–51, 1992.

1052

1053 Gerst, S. and Quay, P.: Deuterium component of the global molecular hydrogen cycle,  
1054 *J. Geophys. Res.*, 106, 5021–5031, doi:10.1029/2000JD900593, 2001.

1055

1056 Gonfiantini, R., Stichler, W., and Rozanski, K.: Standards and intercomparison  
1057 materials distributed by the International Atomic Energy Agency for stable isotope  
1058 measurements, in: Reference and intercomparison materials for stable isotopes of light  
1059 elements: Proceedings of a consultants meeting held in Vienna, 1-3 December 1993,  
1060 IAEA-TECDOC-825, International Atomic Energy Agency, Vienna, 1993.

1061

1062 Guo, R. and Conrad, R.: Extraction and characterization of soil hydrogenases  
1063 oxidizing atmospheric hydrogen, *Soil Biol. Biochem.*, 40(5), 1149–1154,  
1064 doi:10.1016/j.soilbio.2007.12.007, 2008.

1065

1066 Häring, V., Klüber, H. D., and Conrad, R.: Localization of atmospheric H<sub>2</sub>-oxidizing  
1067 soil hydrogenases in different particle fractions of soil, *Biol. Fert. Soils*, 18(2), 109-  
1068 114, doi:10.1007/BF00336455, 1994.

1069



1070 Haumann, F. A., Batenburg, A. M., Pieterse, G., Gerbig, C., Krol, M. C., and  
1071 Röckmann, T.: Emission ratio and isotopic signatures of molecular hydrogen  
1072 emissions from tropical biomass burning, *Atmos. Chem. Phys.*, 13, 9401–9413,  
1073 doi:10.5194/acp-13-9401-2013, 2013.

1074

1075 Heij, G. H. and Erisman, J. W.: Acid Atmospheric Deposition and Its Effects on  
1076 Terrestrial Ecosystems in The Netherlands, *Studies in Environmental Sciences* 69,  
1077 ISBN 0-444-82037-X, Elsevier, Amsterdam, 1997.

1078

1079 Hoffmann, G., Werner, M., and Heimann, M.: The water isotope module of the  
1080 ECHAM atmospheric general circulation model – A study on time scales from days to  
1081 several years, *J. Geophys. Res.*, 103, 16871–16896, doi:10.1029/98JD00423, 1998.

1082

1083 Jordan, A. and Steinberg, B.: Calibration of atmospheric hydrogen measurements,  
1084 *Atmos. Meas. Tech.*, 4, 509–521, doi:10.5194/amt-4-509-2011, 2011.

1085

1086 Kawagucci, S., Toki, T., Ishibashi, J., Takai, K., Ito, M., Oomori, T., and Gamo, T.,  
1087 Isotopic variation of molecular hydrogen in 20°–375°C hydrothermal fluids as  
1088 detected by a new analytical method, *J. Geophys. Res.*, 115, G03021,  
1089 doi:10.1029/2009JG001203, 2010.

1090

1091 Khdhiri, M., Hesse, L., Popa, M. E., Quiza, L., Lalonde, I., Meredith, L. K.,  
1092 Röckmann, T., and Constant, P.: Soil carbon content and relative abundance of high

1093 affinity H<sub>2</sub>-oxidizing bacteria predict atmospheric H<sub>2</sub> soil uptake activity better than  
1094 soil microbial community composition, *Soil Biol. Biochem.*, 85, 1-9,  
1095 doi:10.1016/j.soilbio.2015.02.030, 2015.

1096

1097 Kreuzer-Martin, H. W., Lott, M. J., Ehleringer, J. R., and Hegg, E. L.: Metabolic  
1098 processes account for the majority of the intracellular water in log-phase *Escherichia*  
1099 *coli* cells as revealed by hydrogen isotopes, *Biochemistry*, 45(45), 13622-13630,  
1100 doi:10.1021/bi0609164, 2006.

1101

1102 Luo, Y., Sternberg, L., Suda, S., Kmazawa, S., and Mitsui, A.: Extremely low D/H  
1103 ratios of photoproduced hydrogen by cyanobacteria, *Plant Cell Physiol.*, 32(6), 897–  
1104 900, 1991.

1105

1106 Meredith, L.K.: Field measurement of the fate of atmospheric H<sub>2</sub> in a Forest  
1107 environment: from canopy to soil, Ph.D. thesis, Department of Earth, Atmospheric  
1108 and Planetary Sciences, Massachusetts Institute of Technology, United States, 250 pp,  
1109 2012.

1110

1111 Novelli, P. C., Lang, P. M., Masarie, K. A., Hurst, D. F., Myers, R., and Elkins, J. W.:  
1112 Molecular hydrogen in the troposphere: Global distribution and budget, *J. Geophys.*  
1113 *Res.*, 104, 30427– 30444, doi:10.1029/1999JD900788, 1999.

1114

1115 Pieterse, G., Krol, M. C., Batenburg, A. M., Steele, L. P., Krummel, P. B.,  
1116 Langenfelds, R. L., and Röckmann, T.: Global modelling of H<sub>2</sub> mixing ratios and  
1117 isotopic compositions with the TM5 model, *Atmos. Chem. Phys.*, 11, 7001–7026,  
1118 doi:10.5194/acp-11-7001-2011, 2011.

1119

1120 Pieterse, G., Krol, M. C., Batenburg, A. M., Brenninkmeijer, C. A. M., Popa, M. E.,  
1121 O’Doherty, S., Grant, A., Steele, L. P., Krummel, P. B., Langenfelds, R. L., Wang, H.  
1122 J., Vermeulen, A. T., Schmidt, M., Yver, C., Jordan, A., Engel, A., Fisheraffilmark, R.  
1123 E., Lowry, D., Nisbet, E. G., Reimann, S., Vollmer, M. K., Steinbacher, M., Hammer,  
1124 S., Forster, G., Sturges, W. T., and Röckmann, T.: Reassessing the variability in  
1125 atmospheric H<sub>2</sub> using the two-way nested TM5 model, *J. Geophys. Res.-Atmos.*, 118,  
1126 3764–3780, doi:10.1002/jgrd.50204, 2013.

1127

1128 Popa, M. E., Vermeulen, A. T., van den Bulk, W. C. M., Jongejan, P. A. C.,  
1129 Batenburg, A. M., Zahorowski, W., and Röckmann, T.: H<sub>2</sub> vertical profiles in the  
1130 continental boundary layer: measurements at the Cabauw tall tower in the Netherlands,  
1131 *Atmos. Chem. Phys.*, 11, 6425–6443, doi:10.5194/acp-11-6425-2011, 2011.

1132

1133 Price, H., Jaeglé, L., Rice, A., Quay, P., Novelli, P. C., and Gammon, R.: Global  
1134 budget of molecular hydrogen and its deuterium content: Constraints from ground  
1135 station, cruise, and aircraft observations, *J. Geophys. Res. -Atmos.*, 112, D22108,  
1136 doi:10.1029/2006JD008152, 2007.

1137

1138 Rahn, T., Eiler, J. M., Kitchen, N., Fessenden, J. E., and Randerson, J. T.:  
1139 Concentration and  $\delta D$  of molecular hydrogen in boreal forests: Ecosystem-scale  
1140 systematics of atmospheric  $H_2$ , *Geophys. Res. Lett.*, 29(18), 35-1-35-4,  
1141 doi:10.1029/2002GL015118, 2002a.

1142

1143 Rahn, T., Kitchen, N., and Eiler, J.: D/H ratios of atmospheric  $H_2$  in urban air: results  
1144 using new methods for analysis of nano-molar  $H_2$  samples, *Geochim. Cosmochim.*  
1145 *Ac.*, 66(14), 2475– 2481, doi:10.1016/S0016-7037(02)00858-X, 2002b.

1146

1147 Rahn, T., Eiler, J. M., Boering, K. A., Wennberg, P. O., McCarthy, M. C., Tyler, S.,  
1148 Schaufliker, S., Donnelly, S., and Atlas, E.: Extreme deuterium enrichment in  
1149 stratospheric hydrogen and the global atmospheric budget of  $H_2$ , *Nature*, 424, 918–  
1150 921, doi:10.1038/nature01917, 2003.

1151

1152 Rahn, T., Randerson, J. T., and Eiler, J.: Variability of Deuterium Fractionation  
1153 Associated With Soil Uptake of Atmospheric Molecular Hydrogen, *Eos Trans. AGU*,  
1154 86(52), Fall Meet. Suppl., Abstract B11A-1031, 2005

1155

1156 Rhee, T. S., Mak, J., Röckmann, T., and Brenninkmeijer, C. A. M.: Continuous-flow  
1157 isotope analysis of the deuterium/hydrogen ratio in atmospheric hydrogen, *Rapid*  
1158 *Commun. Mass Spectrom.*, 18(3), 299–306, doi:10.1002/rcm.1309, 2004.

1159

1160 Rice, A., Quay, P., Stutsman, J., Gammon, R., Price, H., and Jaeglé, L.: Meridional  
1161 distribution of molecular hydrogen and its deu- terium content in the atmosphere, J.  
1162 Geophys. Res., 115(D12), 1–12, doi:10.1029/2009JD012529, 2010.

1163

1164 Rice, A., Dayalu, A., Quay, P., and Gammon, R.: Isotopic fractionation during soil  
1165 uptake of atmospheric hydrogen, Biogeosciences, 8, 763–769, doi:10.5194/bg-8-763-  
1166 2011, 2011.

1167

1168 Röckmann, T., Rhee, T. S., and Engel, A.: Heavy hydrogen in the stratosphere, Atmos.  
1169 Chem. Phys., 3, 2015–2023, doi:10.5194/acpd-3-3745-2003, 2003a.

1170

1171 Röckmann, T., Kaiser, J., Brenninkmeijer, C. A. M., and Brand, W. A.: Gas  
1172 chromatography/isotope-ratio mass spectrometry method for high-precision position-  
1173 dependent  $^{15}\text{N}$  and  $^{18}\text{O}$  measurements of atmospheric nitrous oxide, Rap. Commun.  
1174 Mass Spectrom., 17, 1897-1908, 2003b.

1175

1176 Röckmann, T., Álvarez, C. X. G., Walter, S., Veen, C. van der, Wollny, A. G., Gunthe,  
1177 S. S., Helas, G., Pöschl, U., Keppler, F., Greule, M., and Brand, W. A.: Isotopic  
1178 composition of  $\text{H}_2$  from wood burning: Dependency on combustion efficiency,  
1179 moisture content, and  $\delta\text{D}$  of local precipitation, J. Geophys. Res., 115, D17308,  
1180 doi:10.1029/2009JD013188, 2010.

1181

1182 Rothe, M., Jordan, A., and Brand, W. A.: Trace gases,  $\delta^{13}\text{C}$  and  $\delta^{18}\text{O}$  of  $\text{CO}_2$ -in-air  
1183 samples: Storage in glass flasks using PCTFE seals and other effects, in: GAW report  
1184 161,12th WMO/IAEA meeting of experts on carbon dioxide concentration and related  
1185 tracers measurements techniques, edited by: Worthy, D. and Huang, L., Toronto,  
1186 Canada, 15–18 September 2003, WMO TD No. 1275, 2004.

1187

1188 Ruijven, B. van, Lamarque, J. F., Vuuren, D. P. van, Kram, T., and Eerens, H.:  
1189 Emission scenarios for a global hydrogen economy and the consequences for global  
1190 air pollution, *Global Environ. Chang.*, 21(3), 983-994, 2011.

1191

1192 Schmitt, S., Hanselmann, A., Wollschläger, U., Hammer, S., and Levin, I.:  
1193 Investigation of parameters controlling the soil sink of atmospheric molecular  
1194 hydrogen. *Tellus B*, 61(2), 416-423, 2009.

1195

1196 Schultz, M. G., Diehl, T., Brasseur, G. P., and Zittel, W.: Air pollution and climate-  
1197 forcing impacts of a global hydrogen economy, *Science*, 302(5645), 624–627,  
1198 doi:10.1126/science.1089527, 2003.

1199

1200 Smith-Downey, N. V., Randerson, J. T. and Eiler, J. M.: Temperature and moisture  
1201 dependence of soil  $\text{H}_2$  uptake measured in the laboratory. *Geophys. Res. Lett.*, 33,  
1202 L14813, doi:10.1029/2006GL026749, 2006.

1203

1204 Smith-Downey, N. V., Randerson, J. T., and Eiler, J. M.: Molecular hydrogen uptake  
1205 by soils in forest, desert, and marsh ecosystems in California, *J. Geophys. Res.-*  
1206 *Biogeosci.*, 113, G03037, doi:10.1029/2008JG000701, 2008.

1207

1208 Tromp, T. K., Shia, R. L., Allen, M., Eiler, J. M., and Yung, Y. L.: Potential  
1209 environmental impact of a hydrogen economy on the stratosphere, *Science*, 300,  
1210 1740–1742, doi:10.1126/science.1085169, 2003.

1211

1212 Vogel, B., Feck, T., Groß, J. U., and Riese, M.: Impact of a possible future global  
1213 hydrogen economy on Arctic stratospheric ozone loss, *Energy Environ. Sci.*, 5, 6445-  
1214 6452, doi:10.1039/c2ee03181g, 2012.

1215

1216 Vollmer, M. K., Walter, S., Mohn, J., Steinbacher, M., Bond, S. W., Röckmann, T.,  
1217 and Reimann, S.: Molecular hydrogen (H<sub>2</sub>) combustion emissions and their isotope  
1218 (D/H) signatures from domestic heaters, diesel vehicle engines, waste incinerator  
1219 plants, and biomass burning, *Atmos. Chem. Phys.*, 12, 6275–6289, doi:10.5194/ acp-  
1220 12-6275-2012, 2012.

1221

1222 Walter, S., Laukenmann, S., Stams, A. J. M., Vollmer, M. K., Gleixner, G., and  
1223 Röckmann, T.: The stable isotopic signature of biologically produced molecular  
1224 hydrogen (H<sub>2</sub>). *Biogeosciences*, 9(10), 4115-4123, 2012.

1225

1226 Warwick, N. J., Bekki, S., Nisbet, E. G., and Pyle, J. A.: Impact of a hydrogen  
1227 economy on the stratosphere and troposphere studied in a 2-D model, *Geophys. Res.*  
1228 *Lett.*, 31(5), 2–5, doi:10.1029/2003GL019224, 2004.

1229

1230 Xiao, X., Prinn, R. G., Simmonds, P. G., Steele, L. P., Novelli, P. C., Huang, J.,  
1231 Langenfelds, R. L., O'Doherty, S., Krummel, P. B., Fraser, P. J., Porter, L. W., Weiss,  
1232 R. F., Salameh, P., and Wange, R. H. J.: Optimal estimation of the soil uptake rate of  
1233 molecular hydrogen from the Advanced Global Atmospheric Gases Experiment and  
1234 other measurements, *J. Geophys. Res.*, 112, D07303, doi:10.1029/2006JD007241,  
1235 2007.

1236

1237 Yang, H., Gandhi, H., Shi, L., Kreuzer, H. W., Ostrom, N. E., and Hegg, E. L.: Using  
1238 gas chromatography/isotope ratio mass spectrometry to determine the fractionation  
1239 factor for H<sub>2</sub> production by hydrogenases. *Rapid Commun. Mass Spectrom.*, 26(1),  
1240 61-68, doi: 10.1002/rcm.5298, 2012.

1241

1242

1243

1244

1245



1246 **Tables**

1247

1248 Table 1. The deposition velocity ( $v_d$ ), fractionation factor ( $\alpha_{\text{soil}}$ ) as well as its error estimate,  
 1249 and soil cover information for each Speuld experiment (a) and Cabauw net-uptake  
 1250 experiment (b). The STDEV represents standard deviation and SE represents standard error.

1251 The errors of  $\alpha_{\text{soil}}$  represent the 95% confidence interval (CI) for  $\alpha_{\text{soil,app}}$  obtained from

1252  $\ln \frac{c' - c'_{e,\text{app}}}{c'_1 - c'_{e,\text{app}}}$  versus  $\ln \frac{c - c_{e,\text{app}}}{c_1 - c_{e,\text{app}}}$ .

(a)	$F_n$ (nmol m <sup>-2</sup> s <sup>-1</sup> )	$v_d$ (cm s <sup>-1</sup> )	$\alpha_{\text{soil}}$	Error $\alpha_{\text{soil}}$	soil cover
SPU-1	-30.1	0.20	0.924	0.032	D. fir, moss
SPU-2	-35.3	0.22	0.948	0.028	D. fir, needles
SPU-3	-37.7	0.20	0.945	0.008	D. fir, moss
SPU-4	-26.1	0.16	0.913	0.004	D. fir, moss
SPU-5	-24.9	0.16	0.918	0.006	D. fir, moss
SPU-6	-13.2	0.12	0.951	0.031	D. fir, moss
SPU-7	-19.6	0.12	0.939	0.005	beech, leaves
SPU-8	-28.4	0.16	0.955	0.008	<i>Same subsite as SPU-7, leaves removed</i>
SPU-9	-20.4	0.12	0.925	0.002	beech, leaves
SPU-10	-22.3	0.13	0.949	0.060	spruce, moss
SPU-11	-19.4	0.13	0.936	0.068	spruce, needles
SPU-12	-40.5	0.28	0.947	0.004	<i>Same subsite as SPU-11, needles removed</i>
MEAN	-26.5	0.17	0.937	/	/

STDEV	8.2	0.05	0.014	/	/
SE	2.4	0.01	0.004	/	/

1253

1254

(b)	$F_n$ (nmol m <sup>-2</sup> s <sup>-1</sup> )	$v_d$ (cm s <sup>-1</sup> )	$\alpha_{soil}$	Error $\alpha_{soil}$	soil cover
CBW-5	-6.6	0.04	0.943	0.004	few clover, grass
CBW-7	-3.1	0.03	1.019	0.005	few clover, grass
CBW-16	-22.9	0.18	0.993	0.001	bare soil, few grass
CBW-18	-39.3	0.24	0.950	0.054	grass
CBW-19	-7.4	0.14	0.935	0.105	grass
CBW-20	-14.9	0.20	0.940	0.260	bare soil
CBW-25	-8.0	0.12	0.911	0.014	clover, grass
CBW-26	-6.1	0.09	0.916	0.038	grass
MEAN	-13.6	0.13	0.951	/	/
STDEV	12.2	0.08	0.037	/	/
SE	4.3	0.03	0.013	/	/

1255 Table 2. Net flux, deposition velocity and  $\delta D_{\text{soil}}$  (including error) obtained from the mass  
 1256 balance model for the net H<sub>2</sub> emission experiments.

Net emission	$F_n$ (nmol m <sup>-2</sup> s <sup>-1</sup> )	$v_d$ (cm s <sup>-1</sup> )	$\delta D_{\text{soil}}$ (‰)	Error $\delta D_{\text{soil}}$ (‰)
CBW-8	24.5	0.05	-535	53
CBW-10	16.1	0.03	-460	17
CBW-14	13.7	0.02	-629	21
CBW-17	20.3	0.03	-542	1
CBW-21	42.0	0.04	-574	3
CBW-28	150.2	0.14	-488	83
CBW-30	41.0	0.05	-580	7
CBW-31	92.0	0.09	-509	7
CBW-33	46.2	0.10	-451	52
MEAN	49.5	0.06	-530	/
STDEV	44.7	0.04	59	/
SE	14.9	0.01	20	/

- 1 Table 3. Sampling information and the correction coefficients ( $k_{\text{true}}/k_{\text{app}}$ ,  $P_{\text{true}}/P_{\text{app}}$ ,  $\alpha_{\text{soil,true}}/\alpha_{\text{soil,app}}$  and  $(\delta D_{\text{soil,true}}+1)/(\delta D_{\text{soil,app}}+1)$ ) used
- 2 for each experiments. Size S refers to small chamber and size L refers to large chamber.

Exp.	Pressure (kPa)	Flow rate (L min <sup>-1</sup> )	Size	$\Delta t$ (min)	$k_{\text{app}}$ (min <sup>-1</sup> )	$P_{\text{app}}$ (ppb min <sup>-1</sup> )	$k_{\text{true}}/k_{\text{app}}$	$P_{\text{true}}/P_{\text{app}}$	$\alpha_{\text{soil,true}}/\alpha_{\text{soil,app}}$	$(\delta D_{\text{soil,true}}+1)/$ $(\delta D_{\text{soil,app}}+1)$
SPU-1	200	2	S	10	0.199	4.12	1.494	1.601	0.984	/
SPU-2	200	2.2	S	5	0.206	0.67	1.589	7.472	0.998	/
SPU-3	200	3.1	S	5	0.204	3.58	1.496	2.475	0.999	/
SPU-4	200	2.8	S	5	0.160	7.51	1.526	2.136	1.004	/
SPU-5	200	2.6	S	5	0.156	4.16	1.546	2.759	1.004	/
SPU-6	160	3.2	L	5	0.232	7.61	1.184	1.446	0.999	/
SPU-7	160	3.2	S	5	0.128	5.40	1.418	2.264	1.006	/
SPU-8	160	2.5	S	5	0.172	4.23	1.438	2.381	1.001	/
SPU-9	160	2.8	S	5	0.128	4.56	1.440	2.513	1.007	/
SPU-10	180	2.7	S	5	0.128	/	1.502	/	1.005	/
SPU-11	160	2.2	S	5	0.130	/	1.490	/	1.006	/
SPU-12	180	2.3	S	5	0.272	11.30	1.529	1.720	0.994	/
CBW-5	200	2	L	10	0.086	18.24	1.204	1.248	1.001	/
CBW-7	200	1.9	L	10	0.048	11.57	1.260	1.361	0.999	/
CBW-16	210	2.1	S	10	0.183	45.21	1.498	1.505	0.999	/
CBW-18	200	2	S	10	0.240	38.07	1.532	1.527	0.986	/
CBW-19	200	2	S	10	0.145	56.69	1.457	1.463	0.991	/
CBW-20	200	2	S	10	0.196	65.81	1.491	1.494	0.988	/
CBW-25	200	2	S	10	0.122	44.85	1.449	1.460	0.994	/
CBW-26	200	2	S	10	0.088	31.05	1.452	1.475	1.002	/
CBW-8	200	2	S	10	0.044	82.92	1.542	1.438	/	1.048
CBW-10	200	2.6	L	10	0.069	111.00	1.177	1.152	/	1.010
CBW-14	200	2.5	L	10	0.035	82.53	1.251	1.166	/	1.042
CBW-17	220	2.1	L	10	0.047	117.40	1.268	1.198	/	1.024

CBW-21	220	2	L	10	0.078	232.20	1.209	1.179	/	1.008
CBW-28	175	1.8	S	10	0.146	440.90	1.412	1.402	/	1.018
CBW-30	200	2	L	10	0.090	237.70	1.202	1.180	/	1.008
CBW-31	200	2	S	10	0.098	275.10	1.451	1.422	/	1.007
CBW-33	200	2	S	10	0.107	166.50	1.449	1.430	/	1.007

---

3

4

5

6

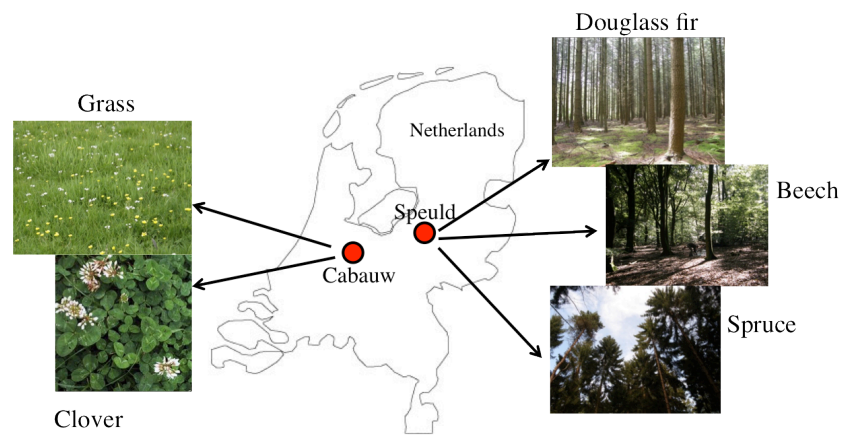
7

8

9

24 **Figures**

25



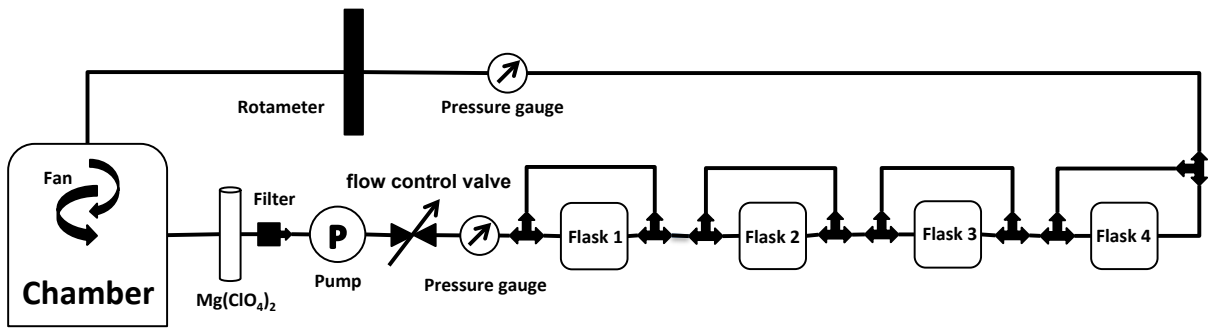
26

27 Fig. 1. The location of the two sampling sites (Cabauw and Speuld) in the Netherlands, as  
28 well as the plant species there.

29

30

31



1285

1286 Fig. 2. Scheme of the sampling setup using the closed-cycle air sampler. The volume of the

1287 soil chamber was 22.8 L and the volume of each flask was 1 L.

1288

1289

1290

1291

1292

1293

1294

1295

1296

1297

1298

1299

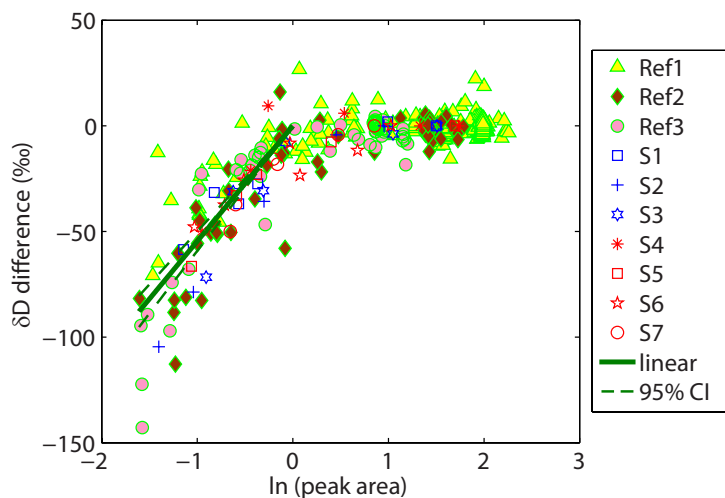
1300

1301

1302

1303

1304



1305

1306 Fig. 3. Difference of  $\delta D$  from the assigned value for different gases including reference gases  
1307 (Ref1-3) and laboratory flask samples (S1-7). A linear function ( $y = 54.6x$ ) was fit to the data  
1308 with peak area between 0.2 and 1.0 V s (green solid line; the dashed lines represent the 95%  
1309 confidence interval of the fit). This function was used to correct the soil experiment data that  
1310 were measured at low peak areas.

1311

1312

1313

1314

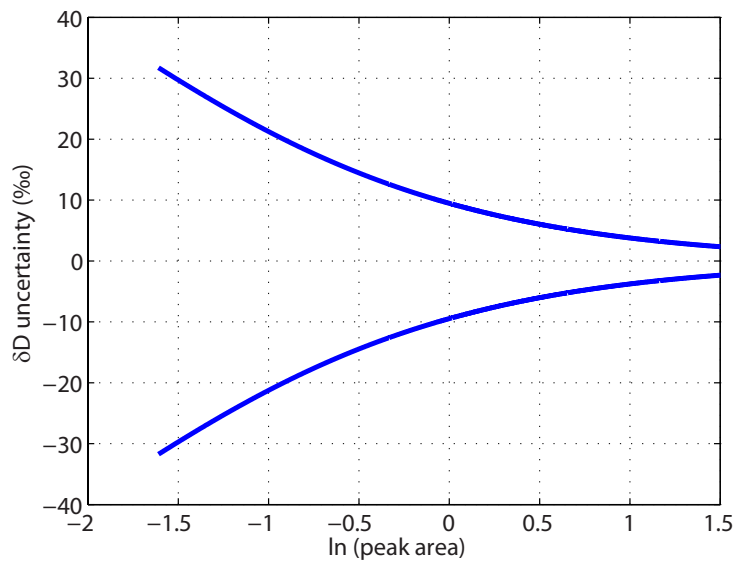
1315

1316

1317

1318





1319

1320 Fig. 4. Calculated total assigned uncertainty of  $\delta D$  (consisting of analytical uncertainty and  
1321 uncertainty arising from the linearity correction) for air samples with  $\ln(\text{peak area})$  ranging  
1322 from -1.6 to 1.5.

1323

1324

1325

1326

1327

1328

1329

1330

1331

1332

1333

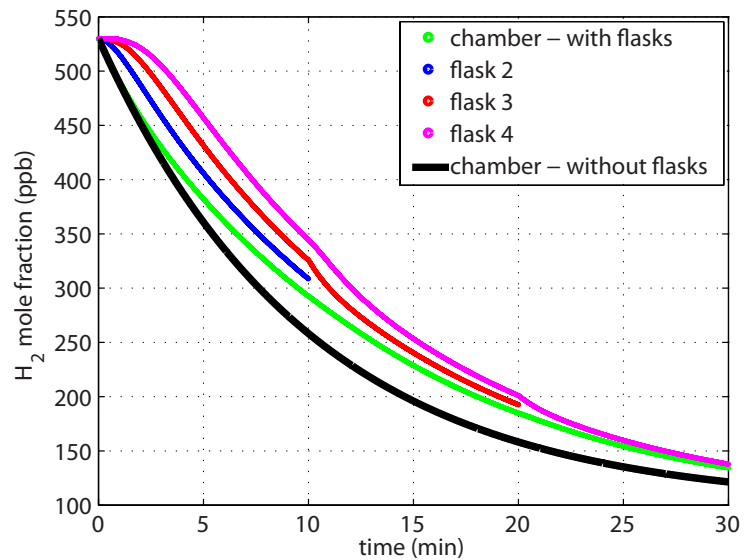
1334

1335

1336

1337

1338



1339

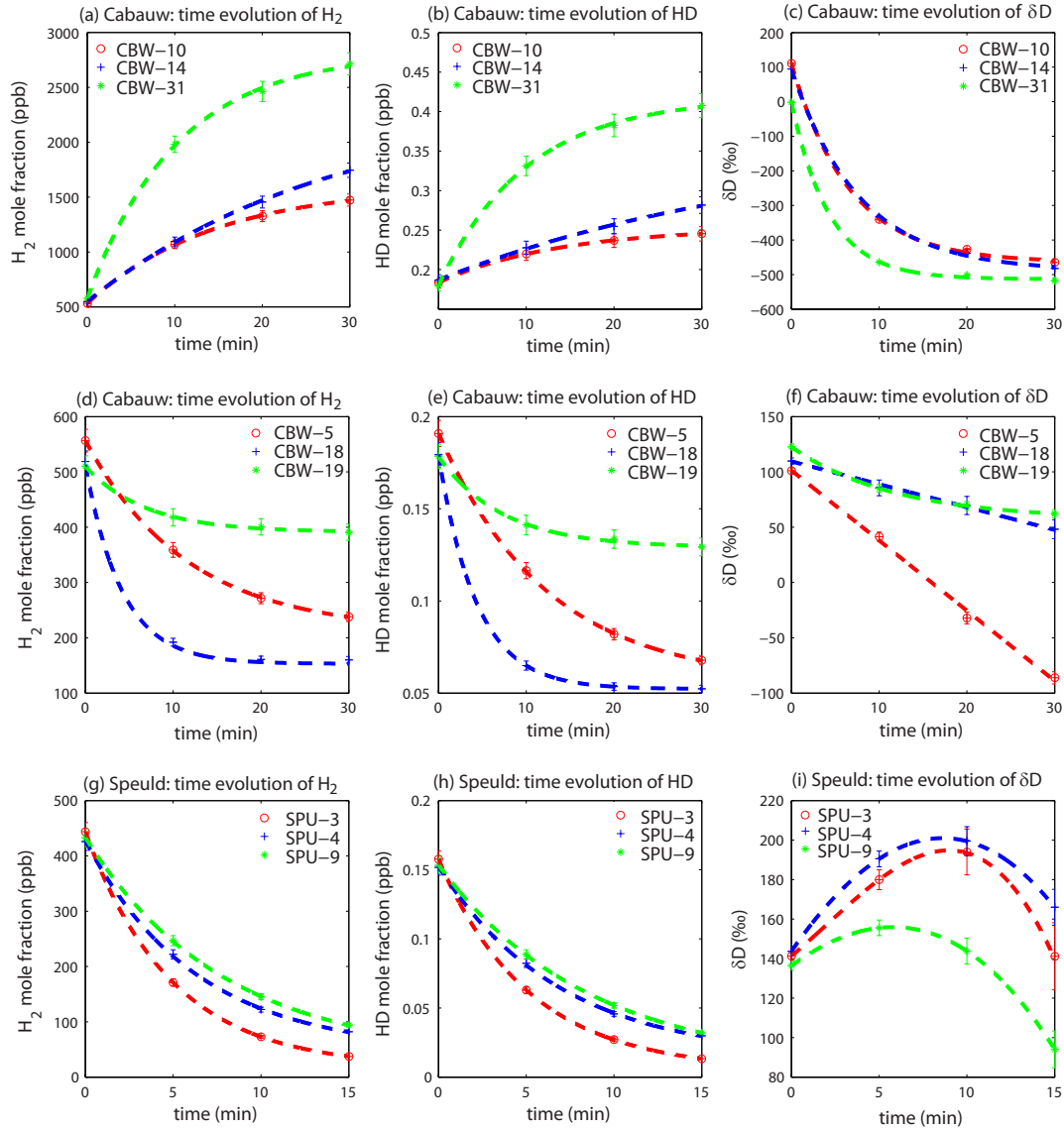
1340 Fig. 5. Results of the flask sampling model with the following parameters:  $k=0.1 \text{ min}^{-1}$ ,  $P=10$   
1341  $\text{ppb min}^{-1}$  and  $c_1(t=0)=530 \text{ ppb}$ . The figure shows the evolution of H<sub>2</sub> mole fraction in the  
1342 chamber (green curve), in flask 2 (blue curve), flask 3 (red curve) and flask 4 (magenta curve)  
1343 as a function of time, and what would be expected for a chamber without flasks (black curve).  
1344 Flask 1 was closed before closing the chamber (at time 0 when all volumes contained the  
1345 same air).

1346

1347

1348

1349

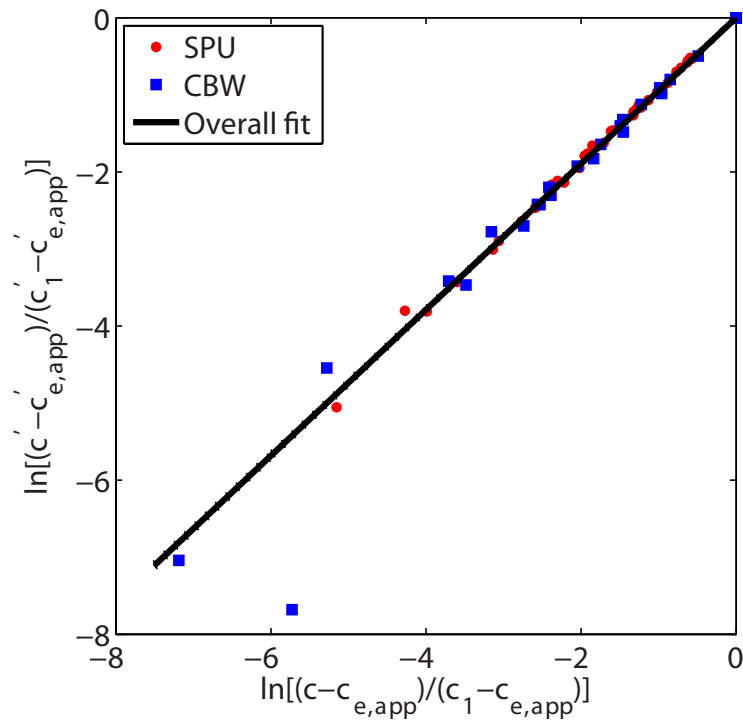


1350  
 1351 Fig. 6. Time evolution of  $H_2$ , HD and  $\delta D$  in Cabauw (upper and middle panels) and in Speuld  
 1352 (lower panel) for representative experiments. HD is calculated from  $H_2$  and  $\delta D$ . The  $H_2$  data  
 1353 are fitted with an exponential function of the form:  $c = (c_1 - c_{e,app})e^{-k_{app}t} + c_{e,app}$ , where  
 1354  $c_1$  and  $c_{e,app}$  are the  $H_2$  mole fractions initially and in equilibrium, and  $k_{app}$  is the apparent soil  
 1355 uptake rate constant for  $H_2$ . A similar exponential function is applied to the HD data. Error  
 1356 estimates for  $H_2$ , HD and  $\delta D$  are shown. The connecting lines for  $\delta D$  data are included to  
 1357 guide the eye.

1358

1359

1360



1361

1362 Fig. 7. Plot of  $\ln \frac{c' - c'_{e,app}}{c_1 - c'_{e,app}}$  versus  $\ln \frac{c - c_{e,app}}{c_1 - c_{e,app}}$  for all Speuld and Cabauw net-uptake  
1363 experiments. The slope of the linear fit to the data returns the fractionation factor  
1364  $\alpha_{soil,app} = 0.947 \pm 0.004$  (95% CI). Errors in x and y direction for each data point were  
1365 considered. One outlier (“CBW-18”) was not included in the fitting. The 95% confidence  
1366 intervals of the fit line are included as dashed lines but largely overlap with the fit line.

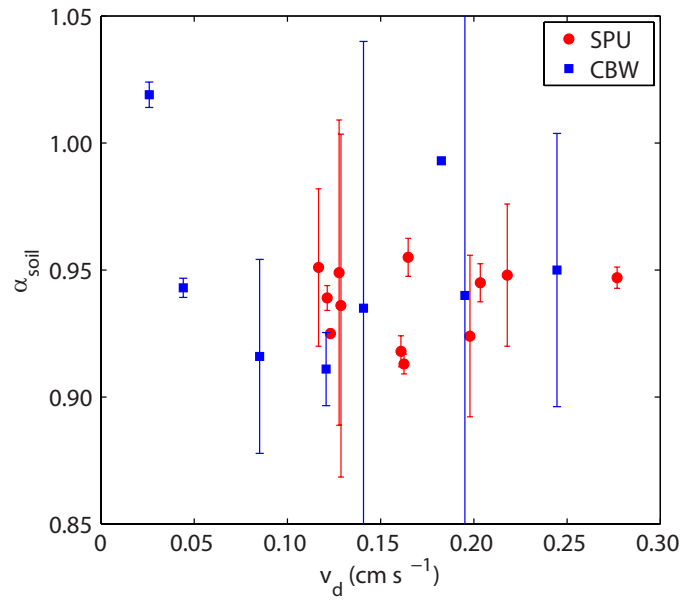
1367

1368

1369

1370

1371



1372

1373 Fig. 8. Correlation between  $\alpha_{soil}$  and  $v_d$  for all Speuld experiments and Cabauw net-uptake

1374 experiments. The errors for  $\alpha_{soil}$  were taken from Table 1.

1375

1376

1377

1378

1379

1380

1381

1382

1383

1384

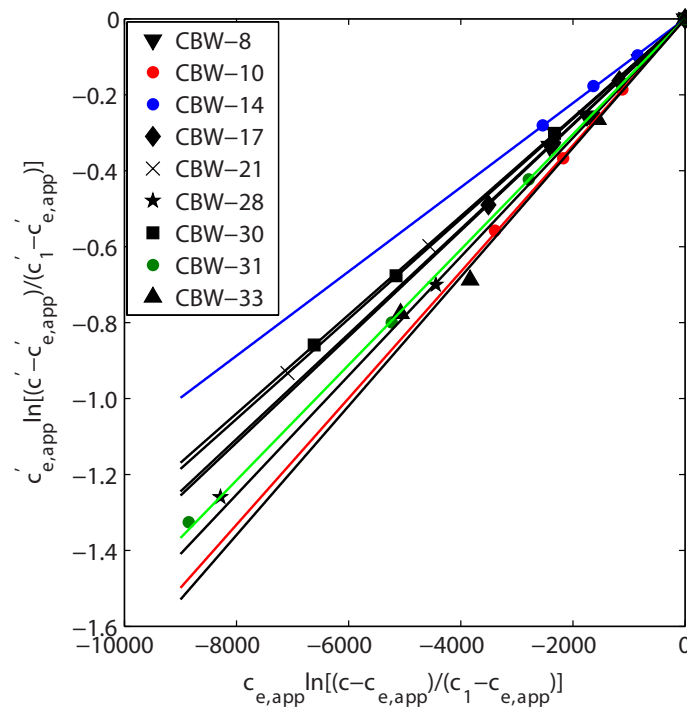
1385

1386

1387

1388

1389



1390

1391 Fig. 9. Plot of  $c'_{e,app} \ln \frac{c' - c'_{e,app}}{c'_1 - c'_{e,app}}$  versus  $c_{e,app} \ln \frac{c - c_{e,app}}{c_1 - c_{e,app}}$  for 9 Cabauw net-emission  
 1392 experiments. A linear function was fit to each individual dataset and the slope was used to  
 1393 calculate the  $\delta D_{soil,app}$  value for each experiment. Errors in x and y direction for each data  
 1394 point were considered.

1395

1396

1397

1398

1399

1400

1401

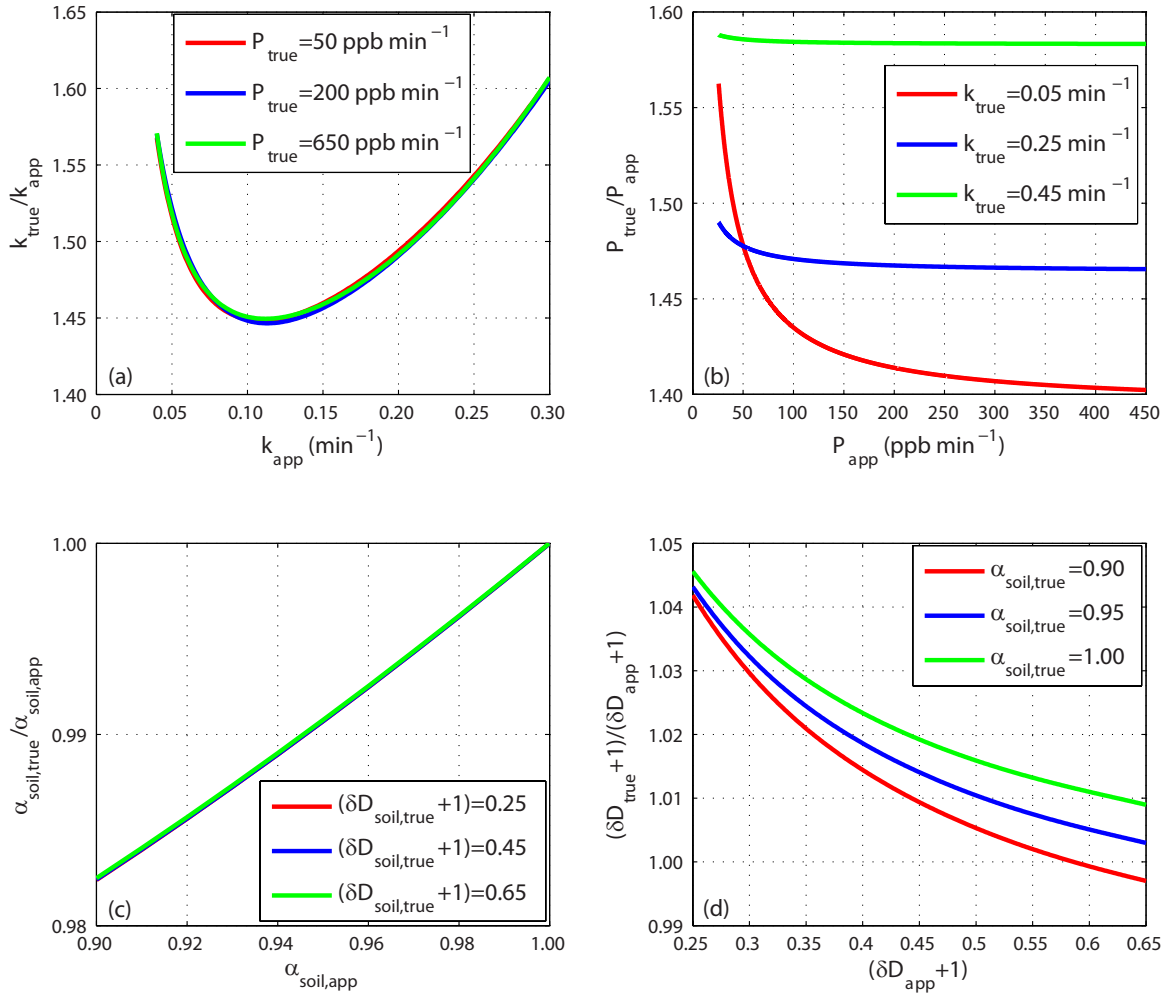
1402

1403

1404

1405

1406



1407

1408 Fig. 10. (a) The relationship between  $k_{\text{true}}/k_{\text{app}}$  and  $k_{\text{app}}$  for  $P_{\text{true}}$  of 50, 200 and 650  $\text{ppb min}^{-1}$ ; (b)

1409 between  $P_{\text{true}}/P_{\text{app}}$  and  $P_{\text{app}}$  for  $k_{\text{true}}$  of 0.05, 0.25 and 0.45  $\text{min}^{-1}$ ; (c) between  $\alpha_{\text{soil,true}}/\alpha_{\text{soil,app}}$  and

1410  $\alpha_{\text{soil,app}}$  for  $(\delta D_{\text{soil,true}} + 1)$  of 0.25 to 0.65 for  $k_{\text{true}} = 0.25 \text{ min}^{-1}$  and  $P_{\text{true}} = 50 \text{ ppb min}^{-1}$ ; (d) between

1411  $(\delta D_{\text{soil,true}} + 1)/(\delta D_{\text{soil,app}} + 1)$  and  $(\delta D_{\text{soil,app}} + 1)$  for  $\alpha_{\text{soil,true}}$  of 0.90 to 1.00 for  $k_{\text{true}} = 0.25 \text{ min}^{-1}$  and

1412  $P_{\text{true}} = 50 \text{ ppb min}^{-1}$ . The parameters of the sampling setup are  $V' = 22.8 \text{ L}$ ,  $f = 2 \text{ L min}^{-1}$ ,  $\Delta t = 10$

1413 min and the pressures inside the flasks and chamber are 200 kPa and 100 kPa respectively.

1414

1415